UNITED NATIONS UNIVERSITY

GEOTHERMAL TRAINING PROGRAMME
Orkustofnun, Grensasvegur 9,
IS-108 Reykjavik, Iceland

Reports 2011
Number 17

INITIAL CONDITIONS OF WELLS OW 905A, OW 907A, OW 913A AND OW 916A, AND A SIMPLE NATURAL STATE MODEL OF OLKARIA DOMES GEOTHERMAL FIELD, KENYA

Vincent Kipkirui Koech
Kenya Electricity Generating Company, Ltd. – KenGen
P.O. Box 785
Naivasha
KENYA
vkoech@kengen.co.ke

ABSTRACT

Olkaria geothermal field has been in exploitation since 1982. The capacity has risen from the initial 15 MWe turbine installed by KenGen to the present combined total of 202 MWe. The rising fuel prices and rising demand of electricity has motivated KenGen to embark on rapid expansion of geothermal electricity generation. Olkaria Domes field received attention with extensive surface exploration ending in 1997 which resulted in the drilling of three deep exploration wells between 1998 and 1999. Production wells have since been drilled in the Domes field with excess steam to support a 140 MWe power plant. In this report, well test data are systematically analysed to obtain information characterizing the reservoir hosting the resource. Also, a brief description is given on surface exploration carried out in the area. Results are unified to a conceptual model of the geothermal system. An upflow zone of more than 300°C is assumed to be in the eastern and south eastern parts of the Domes field, bound within the caldera. The reservoir is two-phase and the upflow temperature and pressure profiles follow the boiling point curves in the wells. Effective permeability of the reservoir ranges from 2.3 to 3.4 mD. The conceptual reservoir model was simulated in a 3 dimensional grid using TOUGH2 simulator, and compared with measured physical data. The volumetric reservoir estimate shows that the field can support more than 210 MWe for a period of 50 years with 90% confidence.

1. INTRODUCTION

The East African Rift system runs from the Afar triple junction at the gulf of Eden in the north to Beira, Mozambique in the south. The Rift Valley divides into two, the Western Rift Valley and the Eastern Rift Valley. The Kenyan rift is the segment of the East African Rift extending from Lake Turkana to Lake Natron in northern Tanzania. Geothermal activity is widespread in many parts of the Kenyan rift; about fourteen geothermal prospects associated with Quaternary volcanic centres occuring in the axial region of the rift have been identified (Omenda, 1998). Drilling has been done in three of these: Olkaria, Eburru and Menengai (Figure 1). The rift is part of a continental divergent zone where spreading occurs resulting in the thinning of the crust and the eruption of lavas and associated volcanic activities (Lagat, 2004).

FIGURE 1: Location map of geothermal prospects in the Kenyan Rift valley

The Greater Olkaria geothermal field (GOGA) is in the southern part of the Kenyan rift. It is located south of Lake Naivasha, approximately 120 km northwest of Nairobi city. The Olkaria geothermal area has been divided into seven development sectors. The sectors (fields) are Olkaria East, Olkaria Northeast, Olkaria Southwest, Olkaria Central, Olkaria Northwest, Olkaria Southeast, and Olkaria Domes. These fields are named with respect to Olkaria Hill (Figure 2).

Exploration for geothermal resources in Kenya started in the 1950's with mainly geological investigations in the region between Olkaria and Lake Bogoria in the northern rift. The exploration resulted in the drilling of two wells, X-1 and X-2, in Olkaria which encountered high temperatures at depth. The exploration then gained momentum with support of the United Nations Development Programme (UNDP). By 1976, six deep wells had been drilled and in 1981 the first 15 MWe generating unit was commissioned. The power plant is in Olkaria East, a part of the Greater Olkaria field. More wells were drilled and connected to the steam gathering system. Unit 2 and Unit 3, each 15 MWe, were commissioned in 1982 and 1985, respectively. Olkaria II, located in Olkaria Northeast, was commissioned in 2003. The plant has been producing 70 MWe since and an additional 35 MWe turbine was commissioned in May 2010, increasing the generation capacity to 105 MWe. Olkaria West hosts Olkaria III Independent Power Producer (IPP) power plant generating 48 MWe; the first 12 MWe unit was commissioned in 2000 and the second with 36 MWe was commissioned in 2009. Total production of GOGA is about 202 MWe.

Surface exploration in the Domes field was completed in 1993 and three deep exploration wells, OW 901, OW 902, and OW 903 were drilled from 1998 to 1999. Production drilling of wells to sustain a 140 MWe power plant has since been completed.

In this report, downhole profiles of temperature and pressure in four Domes field wells (OW 905A, OW 907A, OW 913A and OW 916A) are interpreted to obtain the natural state of the reservoir in the wells' vicinity. Results from tests conducted in the wells are also analysed to characterize the immediate host reservoir and the

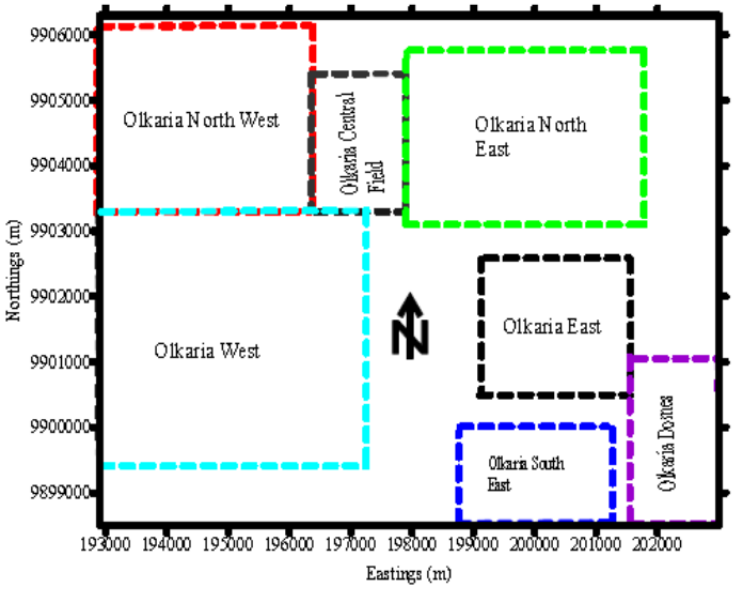

FIGURE 2: Geothermal fields in the Greater Olkaria geothermal area (GOGA) (Opondo, 2007)

individual wells. Previous work was incorporated and an inclusive model developed that forms the basis of a simple numerical model for the natural state that could provide the benchmark, pre-exploitation natural state of the Domes field. The numerical model was then calibrated against the measured field data. Also from the conceptual model, the volumetric method was used to estimate a reserve electricity generating estimate.

2. GEOLOGICAL, GEOCHEMICAL AND GEOPHYSICAL SETTINGS

2.1 Geology

Structural setting: The Olkaria geothermal field is associated with the Olkaria volcanic complex which consists of a series of lava domes and ashes, the youngest of which was dated 2000 years ago (Clarke et al., 1990). The geothermal reservoir is considered to be bounded by arcuate faults forming a ring or a caldera structure. A magmatic heat source might be represented by intrusions at deep levels inside the ring structure. Faults and fractures are prominent in the area with a general trend of N-S and E-W but there are also some inferred faults striking NW-SE. Other structures in the Olkaria area include the Ol'Njorowa gorge, N-S and NW-SE faults, the ENE-WSW Olkaria fault, and WNW-ESE faults (Figure 3) (Muchemi, 2000). Faults are more prominent in the Olkaria East, Northeast and West fields but are scarce in the Domes area, possibly due to a thick cover of pyroclastics. The NW-SE and WNW-ESE faults are thought to be the oldest and are associated with the development of the rift. The most prominent of these faults is the Gorge Farm fault, which forms the boundary of the geothermal fields in the northeast part and extends to the Domes area (Lagat, 1995).

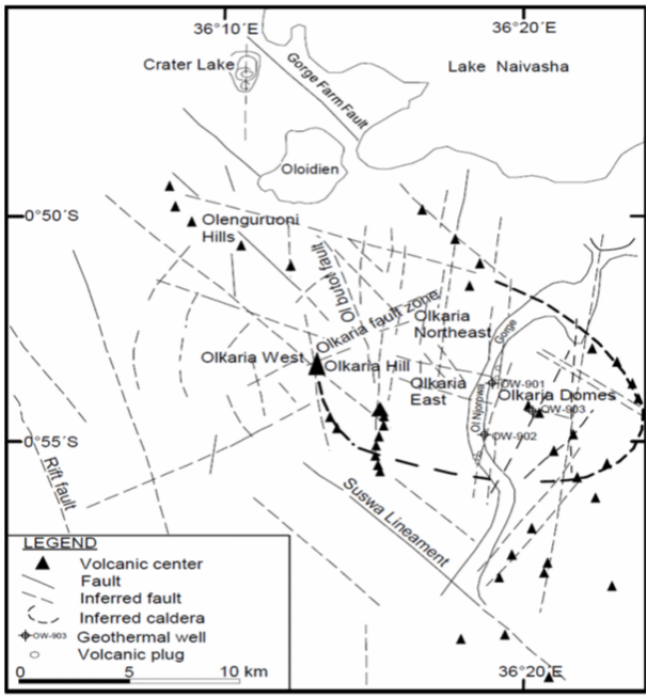

FIGURE 3: Map showing main geological structures of the Greater Olkaria geothermal system (Lagat, 2004)

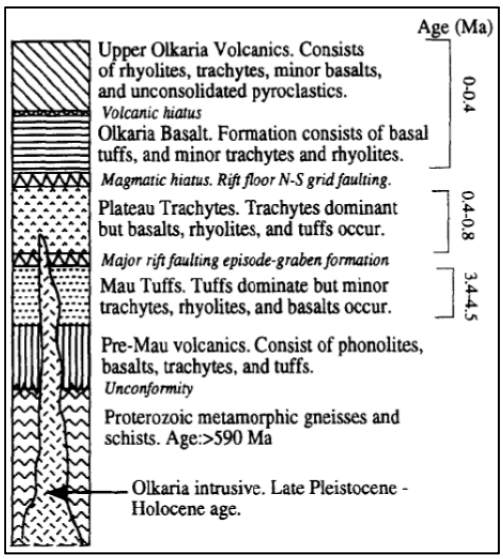

FIGURE 4: Stratigraphic column of the Olkaria volcanic complex (Omenda, 1998)

Stratigraphy: The stratigraphy of the Olkaria area can be described by the exposed lithologic units consisting mainly of volcanic rocks that include comenditic rhyolites, ashes, pumiceous deposits, and trachytes. Lacustrine sediments are rare and occur mostly close to Lake Naivasha. The composition in the subsurface is basalts, trachytes, rhyolites, and tuffs of ages varying from Pliocene to Holocene. A composite stratigraphic column of Olkaria is shown in Figure 4; it is based on data from regional mapping (Naylor, 1972; Shackleton, 1986; Baker, 1987; Clark et al., 1990) and borehole lithological logs.

2.2 Geophysical studies

A wide range of geophysical surveying methods has been employed at Olkaria over the years including seismology, resistivity, gravity, magnetics and electro-magnetics. The compiled resistivity model from the 1-D inversions (Lichoro, 2009) reveals that the Domes well field is generally characterized by a high-resistivity surface layer (> 100 Ωm) which is interpreted as fresh unaltered rocks. Below that is a low-resistivity layer of about 10 Ωm which correlates very well with the mineral alteration of the smectite-zeolite zone of the geothermal reservoir and this, in turn, overlies a high-resistivity core (> 50 Ωm) which is evident in all the cross-sections within the study area. Resistivity at 1000 m b.s.l. (Figure 5) delineates a lower resistivity structure aligned in a NE-SW direction within a high-resistivity core, which could probably be a zone of high permeability where hydrothermal alteration is not advanced, suggesting a possible up-flow zone beneath in a North-South direction along the Domes ring structure.

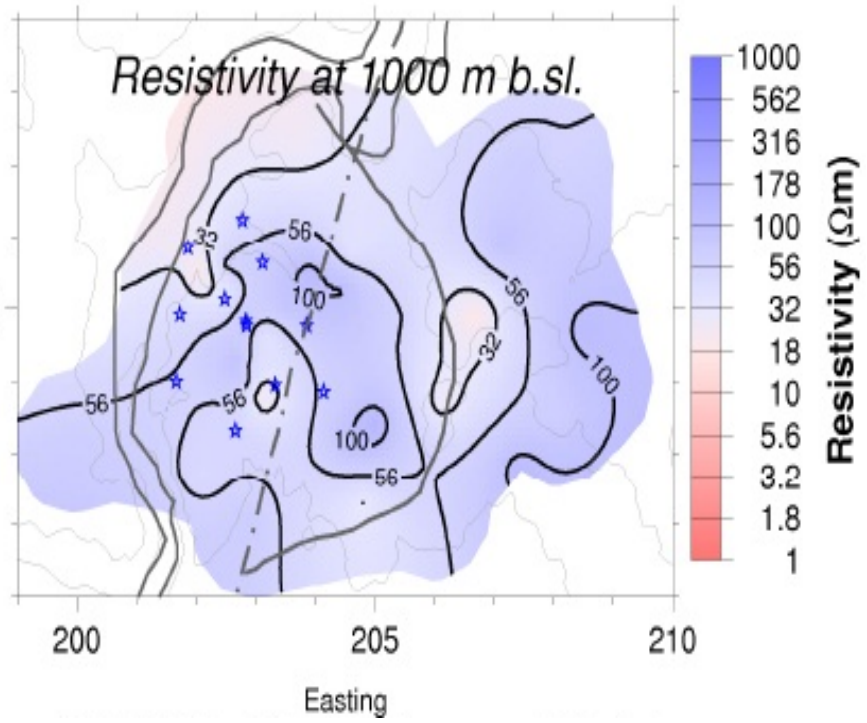

FIGURE 5: Resistivity in the Domes area at 1000 m b.s.l. (Lichoro, 2009)

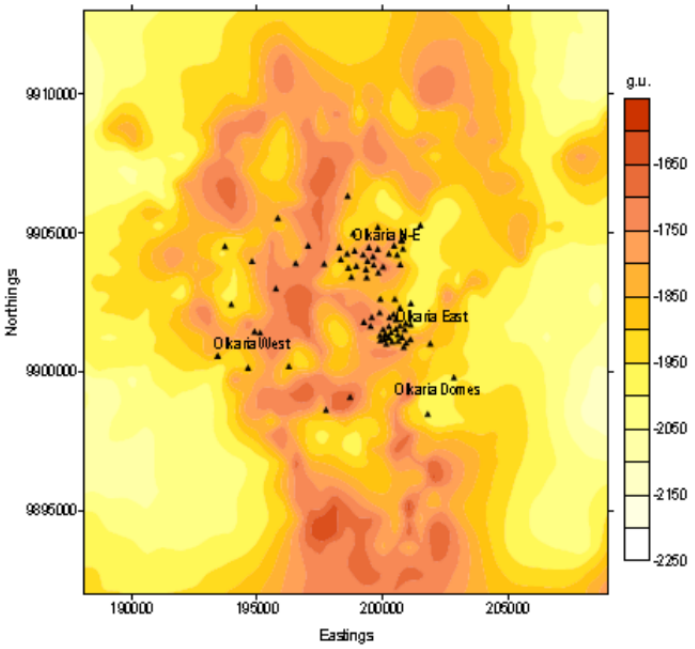

FIGURE 6: Gravity distribution at the Olkaria area (Mariita, 2010)

Results from seismicity and magnetics indicate the presence of attenuating bodies at 6-10 km depth which are also demagnetized within the Olkaria geothermal field (Simiyu et al., 1998; Mwangi and Bromley, 1986). The gravity survey of the shallow crust beneath Olkaria shows a general gravity high trending north-northwest and in line with the regional geological structure in the area (Figure 6). However, there are local highs that trend northeast in line with the recent fault trends and these local gravity highs are interpreted as dyke intrusions which are heat sources in some areas while in others they act as hydrological barriers between fields, e.g. along the Ololbutot fault zone they act as hydrological barriers between the fields. The same can be said for Ol´Njorowa as the chemistry of the fluids for Olkaria Domes differs from the discharge from Olkaria East field.

2.3 Geochemical studies

The studies of geothermal fluid discharged from Olkaria Domes wells by Karingithi (2000) and Malimo (2009) concur on their findings as presented in Figure 7, showing Olkaria Domes wells compared in a comparative plot of relative Cl-SO_4-HCO^3 contents from the discharges of wells in the GOGA fields; the plot illustrates that the geothermal fluids in the Olkaria Domes reservoir are bicarbonate waters and correspond to peripheral waters (Giggenbach, 1991). The figure also shows correlation of the waters with those of the other fields in the GOGA. The Olkaria Domes fluids seem to plot similar to those of Olkaria West and Olkaria Central fields, unlike the wells in the Olkaria East production field and in Olkaria Northeast, which discharge sodium-chloride type water of a mature nature. Solute and gas geothermometry indicate high temperatures in the range of 250-350°C.

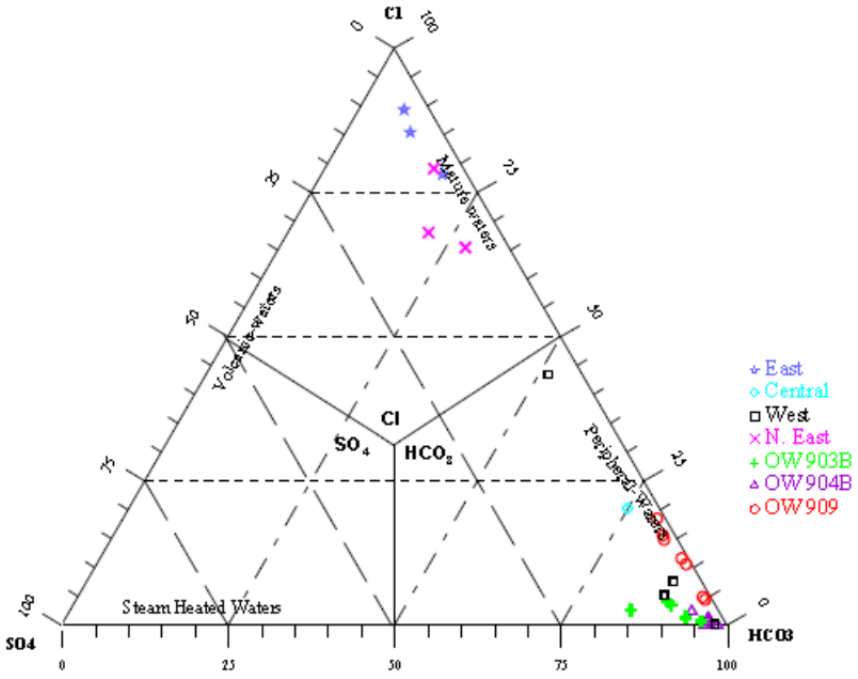

FIGURE 7: Comparative plot of relative Cl-SO_4-HCO_3 contents from the discharges of wells in the GOGA fields (Malimo, 2009)

For the Domes field wells, there is low calcium concentrations and high pH; calcite scaling can, thus, be expected to be minimal in these wells but the fluid has to be separated at temperatures above 100°C to prevent silica scaling.

3. FORMATION TEMPERATURE AND INITIAL PRESSURE OF WELLS OW 905A, OW 907A, OW 913A AND OW 916A

Understanding a potentially useful geothermal resource and its properties is important. Geothermal well logging would be a worthwhile investment as it would provide some of that information. Table 1 gives a description of the selected wells.

TABLE 1: Location and description of wells in the Olkaria Domes

Well no.	Total drilled depth (m)	Easting (m)	Northing (m)	Elevation (cellar top) (m a.s.l.)	Production casing elevat. (m a.s.l.)
OW 905A	2800	202777.75	9901245.5	1946.93	677.92
OW 907A	2581	203113.00	9900635.8	1972.09	805.00
OW 913A	3010	202341.87	9899117.5	1979.63	820.17
OW 916A	3000	204879.24	9899063.8	2034.43	1088.00

3.1 Temperature and pressure profiles

The most common downhole measurements made in geothermal wells are temperature and pressure logs. These are normally measured over the full depth of the wellbore with the well remaining in the same condition throughout the run while stopping the logging tools at intervals of 50 m. The conditions the well is in can be different, closed, flowing or in the process of being injected. Temperature and pressure logging in the Olkaria Domes was done using Kuster mechanical tools starting from the time drilling was completed, while the wells were heating up, discharging and when the wells were shut in. Measurements were also done while the wells were heating up after shut in.

The wells and the surrounding rock are cooled down during drilling by using drilling fluid. It takes some time for a formation to recover its initial temperature. Increase in wellbore temperature can be the result of heat conduction from the surrounding formation, outflow from one feed into another feed in the wellbore, convection within the wellbore, cross flow across the wellbore and also there could be cooling due to boiling during well discharge. Formation temperature and initial pressures serve as the base for conceptual and numerical models. Temperature recovery measurements after drilling were used to estimate formation temperature with the Horner method using computer program BERGHITI (Arason et al., 2003) which assumes that conduction is the dominant mechanism of heat transfer. A Horner plot was used for analysing formation temperature at a given depth using a straight line relationship between the temperature at that particular depth and $\ln(\tau)$, where:

$$\tau = \left(\frac{t_0 + \Delta t}{\Delta t}\right) \tag{1}$$

τ is the Horner time, t_o is the circulation time (duration of circulation) and Δt is the time passed since circulation stopped. As $\lim \Delta t \rightarrow \infty$ this shows that $\ln(\tau) = 0$ and therefore, it is possible to determine the formation temperature from the straight line on a semi logarithmic plot of temperature as a function of the Horner time. Temperatures at different depths can be approximated and a profile then drawn.

The downhole pressure is usually controlled by one feed zone in a well where the feed is dominant and is representative of the formation pressure at the feed zone elevation. Pressure logs are also used to determine the pivot point in a well during the warm-up period; as the fluid in a well warms up, the pressure profiles will pivot about this point of the pressure profile. This usually occurs at the strongest aquifer in the well and is difficult to determine later during production (Stefánsson and Steingrímsson, 1990). If the well has two major feed points, the pivot point will appear between them (Grant et al., 1982). BOILCURV, a computer program for generating the boiling point with depth curves, and PREDYP program for calculating pressure in a static water column when the temperature is known (Arason et al., 2003) were used where appropriate to estimate the initial conditions.

OW 905A: Well OW 905A was cased down to 678 m a.s.l. In Figure 8, from the surface to 1600 m a.s.l., temperature profiles did not change with depth, interpreted as cold shallow groundwater least interfered with. The injection profile temperature also did not change with depth from the surface to 550 m a.s.l. where there was a gradual gradient change followed by another gentle change at 250 m a.s.l. The profiles had a steep gradient below -500 m a.s.l. to the well bottom, suggesting conductive heating in this interval. All the heat-up profiles had almost constant temperature with depth, characteristic of convective heating between depths 550 m a.s.l. and -500 m a.s.l. The slight break in gradient in the profiles between depths -250 and -500 m a.s.l. suggests inflow from a feed at 550 m a.s.l. and outflow from the well in feeds at -250 m a.s.l. and -500 m a.s.l. The pressure profiles, seen in Figure 8, pivot at 550 m a.s.l. and, as noted from the temperature profiles, the main feed zone is at this depth. The estimated formation temperature and initial pressure are shown with a black line in Figure 8. Estimates from BERGHITI are shown in purple dots.

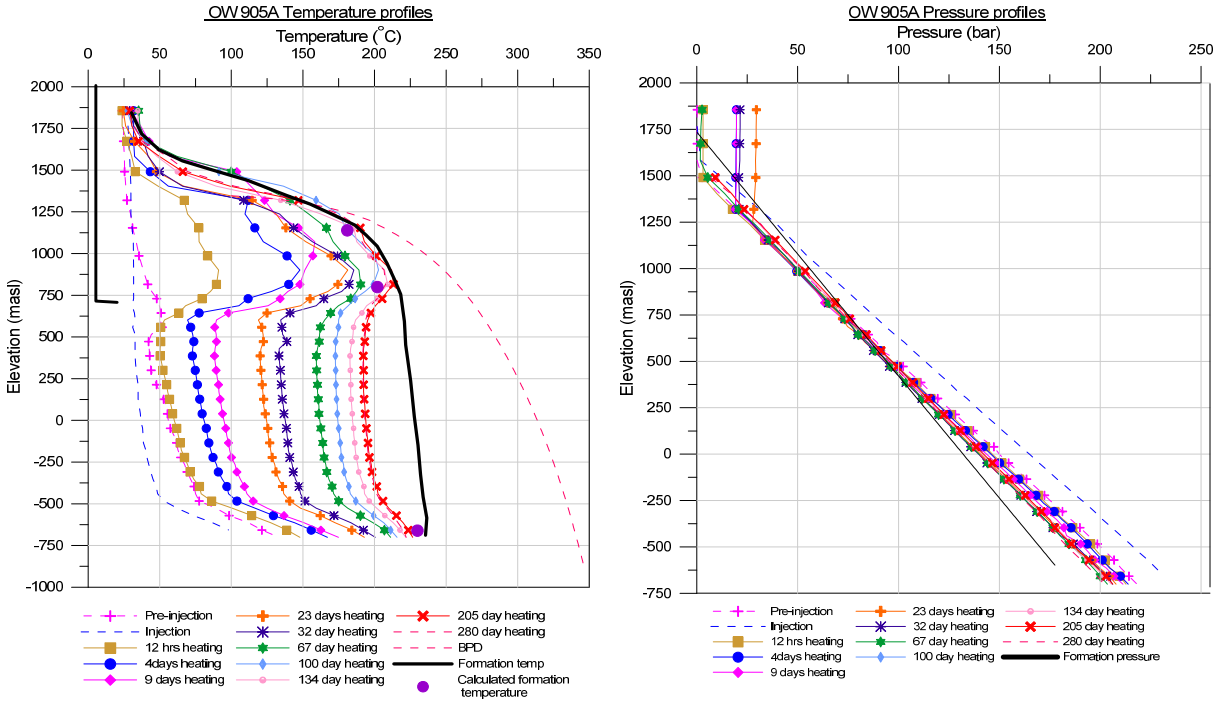

FIGURE 8: Well OW 905A temperature profiles (left) and pressure profiles (right)

OW 907A: The heat up profiles in well OW 907A (Figure 9) indicated conductive heating from the surface to 1200 m a.s.l. Although cased off, there is a convective zone at 1200-950 m a.s.l. (casing shoe at 805 m a.s.l.). In the pre-injection profile an inversion was noted at 750 m a.s.l., indicating permeability as this point was cooled by drilling fluids and another feed at 125 m a.s.l. where there was a break in the temperature gradient. In all the heat up profiles, there was slow recovery at region 750-700 m a.s.l., confirming the presence of a feed zone. Temperature did not change with depth in profiles at depths between 600 and 250 m a.s.l. and from 150 m a.s.l. to the well bottom, suggesting

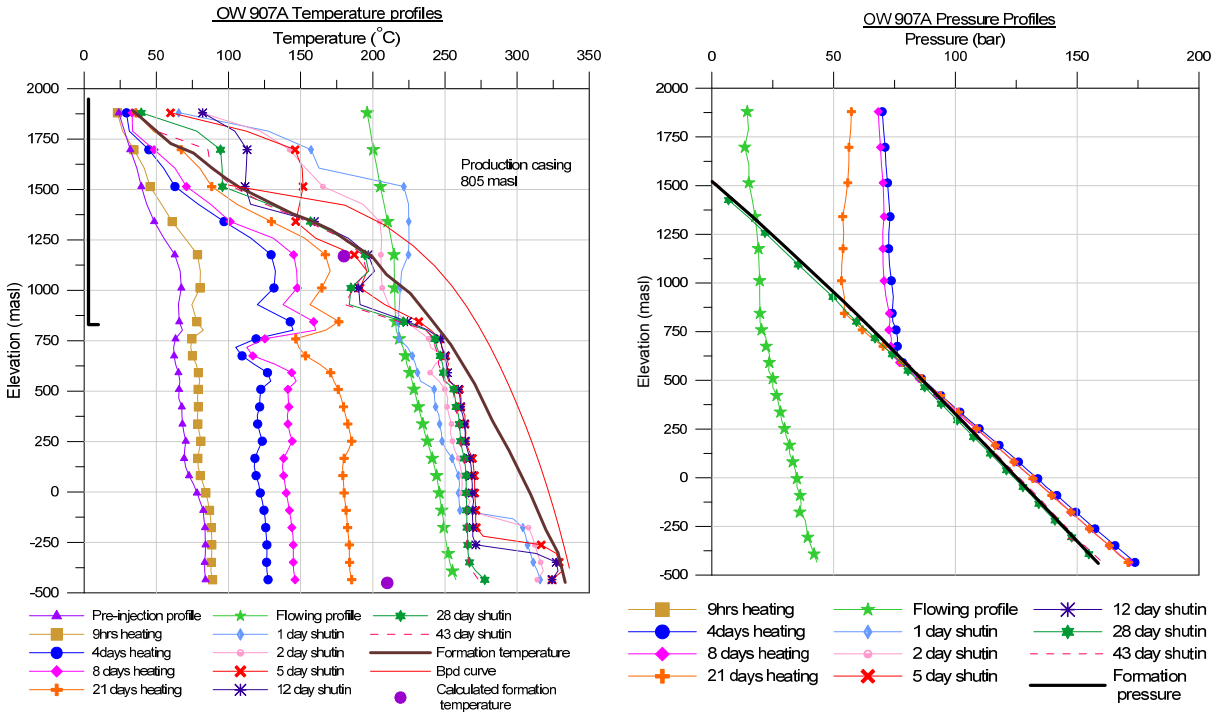

FIGURE 9: Well OW 907A temperature profiles (left) and pressure profiles (right)

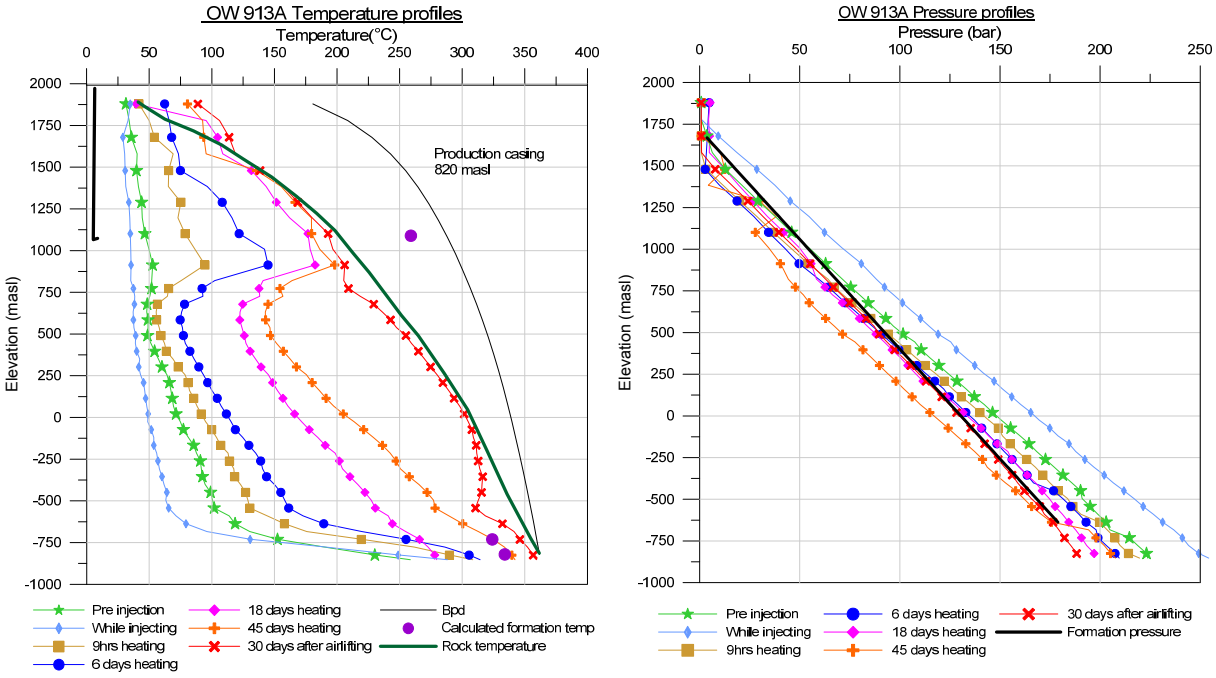

FIGURE 10: Well OW 913A temperature profiles (left) and pressure profiles (right)

the presence of convection. The pressure profile pivoted at 500 m a.s.l. and, as there were no pronounced effects of a feed at this depth, it could be interpreted as a balance between the feed at 700 m a.s.l. and the ones below 125 m a.s.l.

OW 913A: The well was cased off down to 820 m a.s.l. The temperature profile (Figure 10) taken during injection had a small step rise in temperature at 810 m a.s.l., indicating some fluid inflow into the well at 620 m a.s.l.; at 0 m a.s.l. there was a small gradient change with temperature rise down the well and, at -550 m a.s.l., there was a steep rise in temperature to the well bottom, indicating most of the injected water went to the formation above this point. Small feed zones could be inferred to exist at 810 and 0 m a.s.l. and larger feeds at 620 and -550 m a.s.l., as noted from the injection profile. Pre-injection and subsequent downhole profiles indicated linear rise in temperatures with depth from the surface down to 850 m a.s.l., characteristic of conductive heating in the cap rock. Between depths 750 and 500 m a.s.l., there was slow recovery that could be attributed to convection of cooler fluid in this zone or the presence of inter-zonal flow between the feeds. From 500 to -500 m a.s.l., and at -500 m a.s.l. to the well bottom, the profiles had a linear change in temperature with depth which is characteristic of conductive heating. The steep gradient from -500 m a.s.l. to the well bottom indicated that the well did not accept injected fluids and thus was not cooled, whereas for depths 500 to -500 m a.s.l., there was rapid recovery at -500 m a.s.l. The injection pressure log (Figure 10) showed pressure build-up in the well, predicting low permeability. The pressure profiles did not have a definite pivot point but there was convergence at 625 m a.s.l. Initial pressures were calculated with PREDYP.

OW 916A: In well OW 916A (Figure 11), the well was cased off to 1088 m a.s.l. Right below the casing shoe there was a gentle rise in the injection temperature profile, indicating the possibility of a feed zone at 1000 m a.s.l., and between 0 and -625 m a.s.l., where there was a broad but poorly defined zone of injected fluid loss. A feed zone was located at 0 and -373 m a.s.l. From -650 m a.s.l. to the well bottom, the profile was linear and most feeds were located above. Later heating profiles indicated convective heating between depths 1000 and 0 m a.s.l. The influence of conductive heating manifested in 13 and 37 day heating profiles in the region from 0 m a.s.l. to the well bottom. The pressure profiles did not show a unique pivot point (Figure 11). The temperature profiles taken while the well was still recovering were used through the Horner method to estimate the formation temperature. The formation temperature follows the boiling point with depth curve, and it is from this

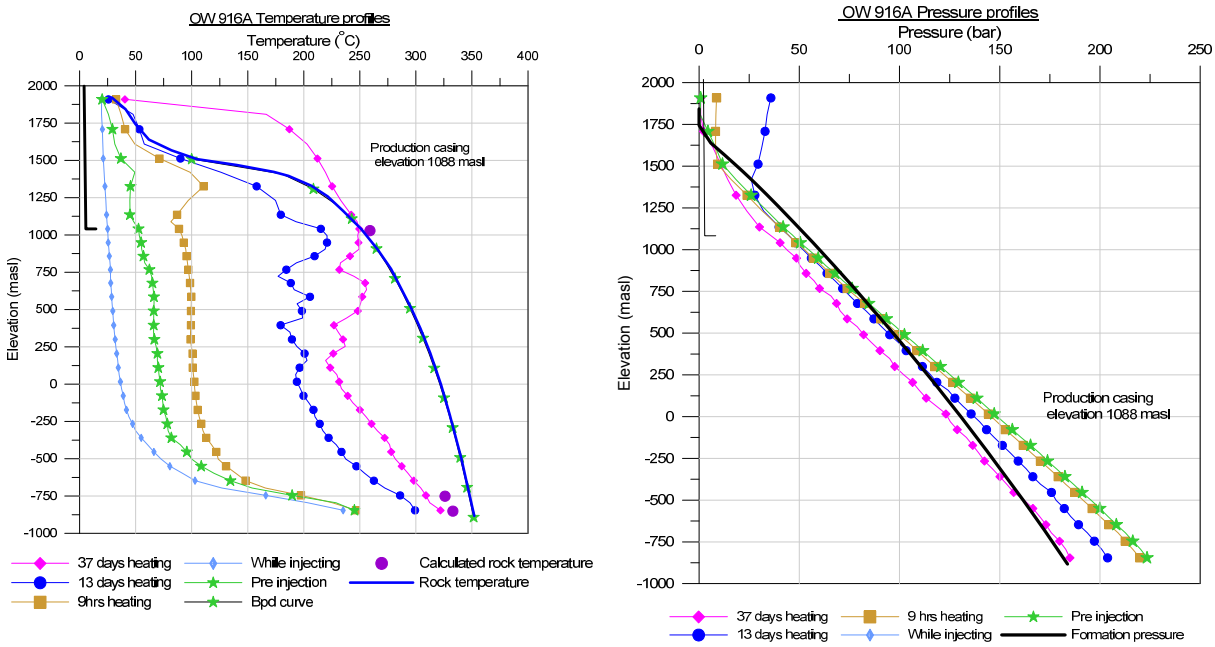

FIGURE 11: Well OW 916A temperature profiles (left) and pressure profiles (right)

that the saturation pressure, obtained using PREDYP program, was taken for the estimated formation pressure.

In all four wells the temperature profiles had conductive heating from the surface to varied depths, interpreted as caprock which is found down to different elevations. The steep conductive gradients noted in wells OW 913A and OW 916A could be an indication of a close heat source. The bottomhole temperatures were: OW 905A with 225°C; OW 907A with 325°C; OW 916A with 325°C; and OW 913A recording the highest at 357°C. Formation temperatures were also estimated using the Horner method with the BERGHITI program for all the wells. The method estimated well the formation temperature for OW 916A, and OW 905A as there were sufficient recovery logs, while for well OW 907A there were not enough logs. BERGHITI estimated formation temperatures are plotted as dots in the Figures showing the temperature profiles.

3.2 Temperature and pressure model

In a geothermal system in the natural state with a hot exploitable part, there has to be an aquifer or a channel network containing hot fluid, a path that cold water can flow down to maintain the through flow, a source of heat, and there could also be an aquiclude or a caprock (Grant et al., 1982). Upflows distinguish a geothermal system from a groundwater system as the pressure drive that sustains the upflows is the buoyancy difference between columnar or ascending hot fluid and descending cold fluid. The buoyancy effects may be supplemented or reduced by topographical effects. In the reservoir, upflows are locally affected by the hydrogeological structures of the reservoir which, in turn, control the heat distribution. Thus, in order to develop a conceptual reservoir model, the estimated formation temperatures for the analysed wells were used together with data on wells in the Domes field covered by earlier studies (Kariuki, 2003; Mwarania, 2010; Odeny, 1999; and Ofwona, 2002). Figure 12 shows a map of the Olkaria Domes field with well locations and locations of cross-sections. Temperature and pressure sections showing areal and vertical distribution in the Domes field were plotted to conceptualize a model.

Figure 13 shows the horizontal temperature and pressure distributions at 1000 m a.s.l. A low-temperature zone runs N-S through the middle of the field; the hottest zone is to the east and southeast. Pressure potential at the same elevation shows high potential to the northeast.

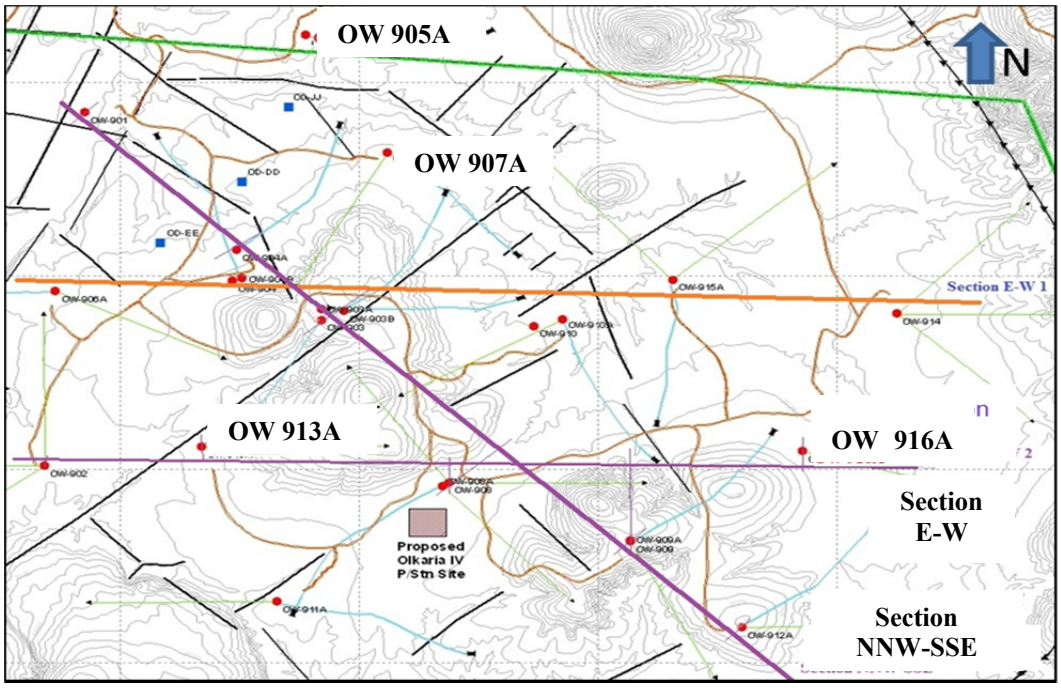

FIGURE 12: Map of Olkaria Domes field showing well locations and the two cross-sections E-W and NNW-SSE

At sea level (Figure 14) the hot zone to the east aligns N-S and covers a larger area to the east. Another hot zone from the centre to the N-W manifests. The cold zone is restricted to the northern and southern parts of the field. Also, in the pressure contours, high pressure potential is shown north of the field, gradually reducing to the east and south but reducing more rapidly to the west. The high pressure and low temperature to the north are interpreted as the field's boundary.

At -600 m a.s.l. (Figure 15) a hot zone of heat covers a larger area; the hot zone to the west is not clearly defined as there are few wells at this depth, for the three exploration wells on this side of the field are shallow. The cold zone is now restricted to the north.

The horizontal pressure distribution at 1000 m a.s.l. (Figure 13) shows high potential to the east and a low pressure region to the southwest towards OW 902. The concurrence of high temperature and high pressure potential to the east of the field suggests an upflow surrounded by OW 909A, OW 910 OW 915A and OW 916. The pressure isobars at -600 m a.s.l. (Figure 15) show high pressure on the

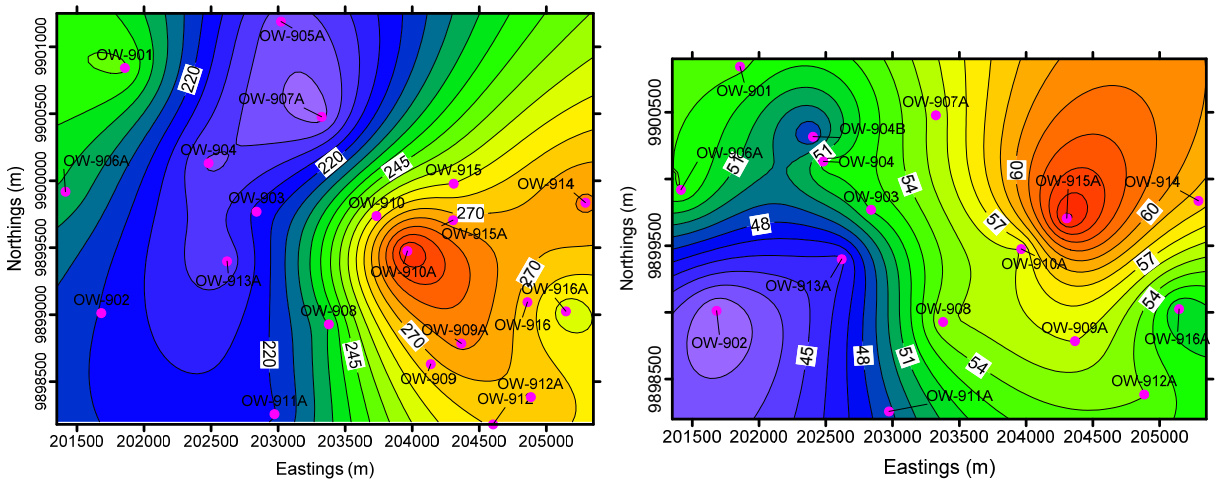

FIGURE 13: Horizontal distribution of temperature (°C) (left) and pressure in bar (right) at 1000 m a.s.l.

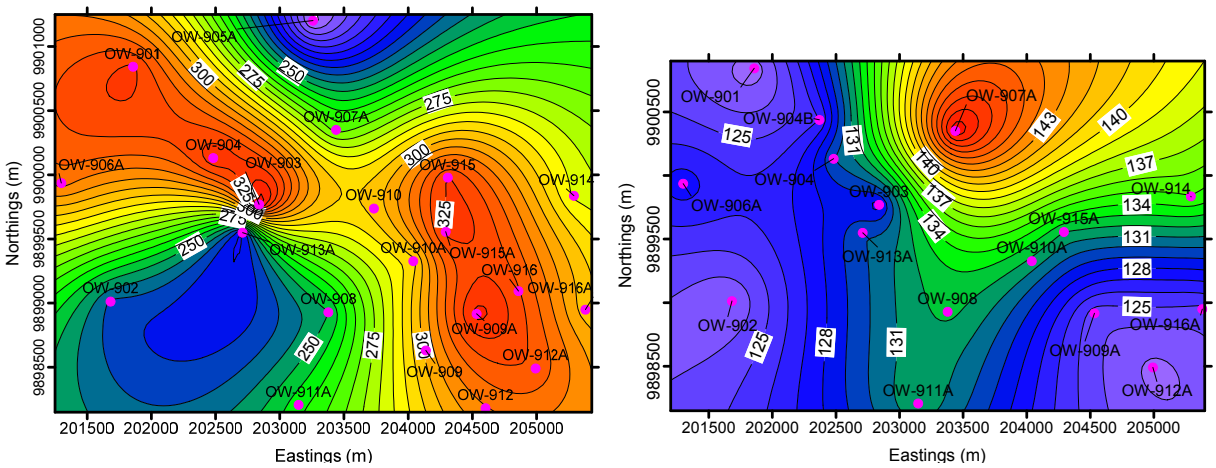

FIGURE 14: Horizontal distribution of temperature (°C) (left) and pressure in bar (right) at sea level

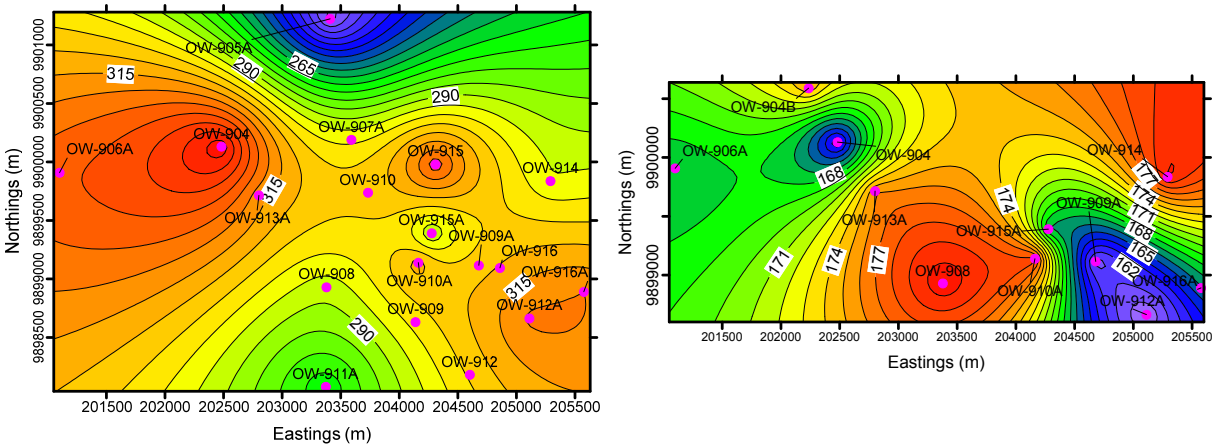

FIGURE 15: Horizontal distribution of temperature (°C) (left) and pressure in bar (right) at -600 m a.s.l.

eastern side of the field, except for the southeast part of the field which showed low pressure. Generally, the pressure isobars show pressure potential to be high in the northeast part of the field reducing in a south-westerly direction.

A vertical cross-section of temperature in a NNW-SSE direction is shown in Figure 16. There is a hot plume between OW 909A and OW 912, but temperature reduces to the north-northwest where the

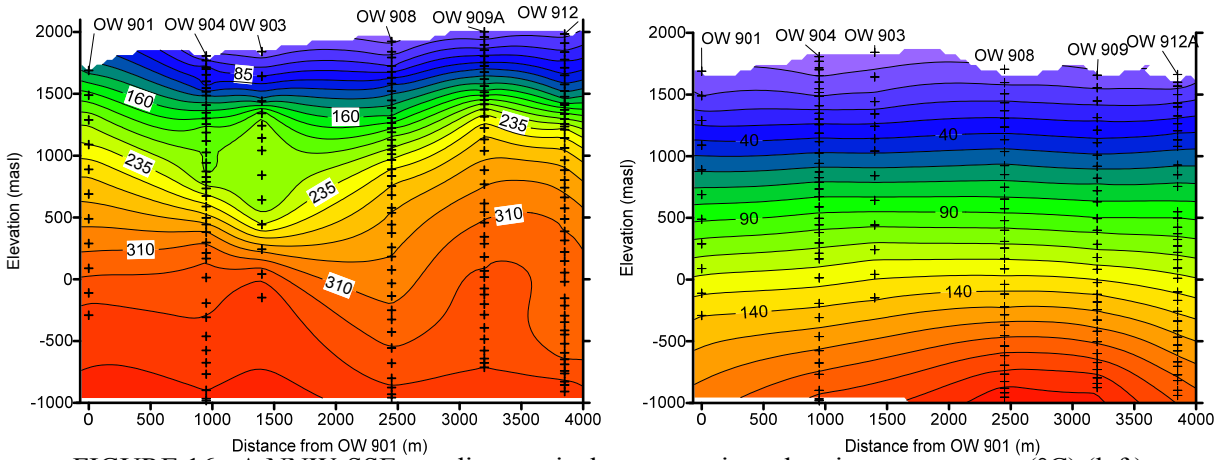

FIGURE 16: A NNW-SSE trending vertical cross-section, showing temperature (°C) (left) and pressure (bar) (right); see Figure 12 for location of cross-section

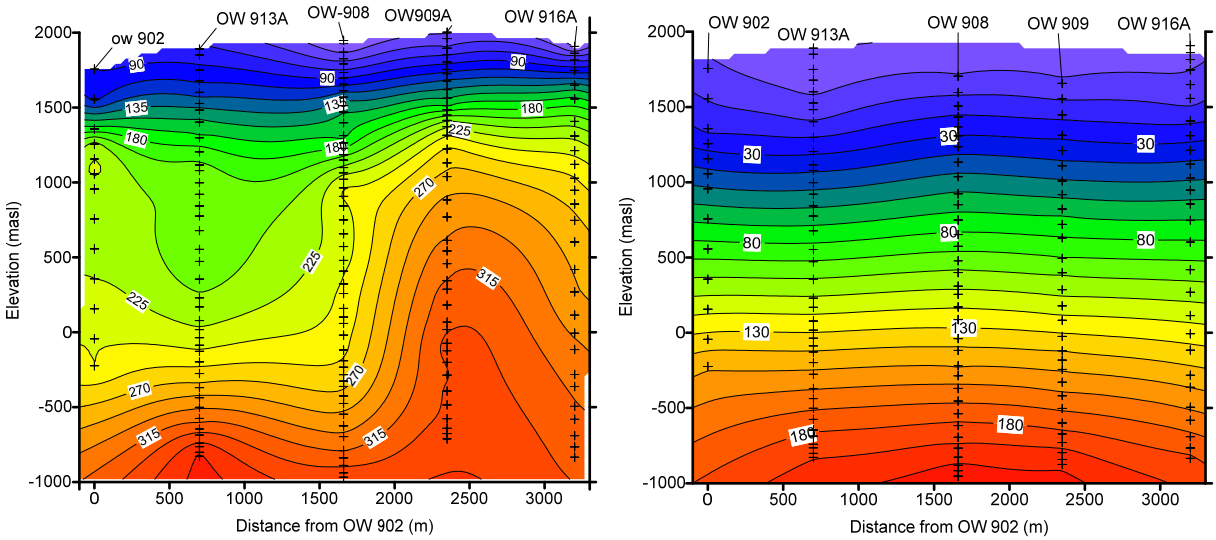

FIGURE 17: A E-W trending vertical cross-section, showing temperature (°C) (left) and pressure (bar) (right); see Figure 12 for location of cross-section

temperature gradient is almost linear with depth and conductive towards OW 901. South-southeast in the profile at shallow depth, the temperature gradient is high and conductive in nature below which there is convection. The vertical pressure cross-section in Figure 16 suggests that in the area around OW 909 and OW 908 there is high pressure potential at depth, but at shallow depth the isobars are almost horizontal. In the E-W vertical cross-section running from OW 902 to OW 916A (Figure 17) there is a hot plume around OW 909A and OW 916A, to the east of the field.

From the cross-sections of temperature and pressure distributions presented above, upflow is inferred to be in the area bounded by OW 909A, OW 910, OW 915A, and OW 916 towards the east and southeast. These wells follow closely the BPD curves, which is characteristic of wells located close to an upflow area.

4. TESTING OF WELLS OW 905A, OW 907A, OW 913A AND OW 916A

Knowledge of the properties of the reservoir hosting the resource is required for effective utilization. Decisions on ways to exploit the source greatly depend on the information known about the reservoir. Injection tests, discharge tests, and shut in tests are performed to obtain information that characterizes the system. In a pressure transient test, the pressure response to the imposed disturbance in a well is monitored as production or injection is changed in order to evaluate the properties that govern the nature of the reservoir. This response is indicative for the characteristic of flow or deliverability properties of the reservoir. The properties include transmissivity, storativity, and wellbore storage and skin among others, and are evaluated using models that are based on the pressure diffusion equation.

4.1 Injection tests

These are pressure transient tests where cold water is injected at different rates, thus causing pressure disturbances; the reservoir response is then monitored. The data obtained are used in a mathematical model that relates pressure responses to flow rate history. Since the response is a characteristic of the reservoir, properties can be inferred from the observed response.

4.1.1 Pressure diffusion equation

The pressure diffusion equation is derived from the conservation law of mass, conservation of momentum and the equation of the state of the fluid, and is the basis for models used in well test interpretation. The equation describing isothermal flow of a fluid in a porous media, how the pressure (p) diffuses radially through the reservoir as a function of the distance (r) from the well and the time (t) since the start of production at rate Q is obtained by solving the pressure diffusion equation. This is achieved by using applicable initial and boundary conditions to a particular case. To simplify the derivation, the following assumptions on the reservoir and flow are used:

a) Reservoir is considered homogenous, isotropic, extends to infinity and has uniform thickness;
b) Flow is considered isothermal and radial;
c) Flow is based on single-phase saturated liquid with small compressibility;
d) Well fully penetrates the entire formation thickness and the radius of the well bore is negligible.

Laws governing the diffusion equation

Law of conservation of mass: Consider a cylindrical control volume around the well and apply conservation of mass:

Mass flow in – mass flow out = mass rate change within the control volume

or

$$\rho Q - \left[\rho Q + \frac{\partial(\rho Q)}{\partial r}\partial r\right] = 2\pi r \frac{\partial(\varphi \rho h)}{\partial t} \tag{2}$$

Darcy's law (conservation of momentum):

$$Q = -\frac{2\pi r h k}{\mu}\frac{\partial p}{\partial r} \tag{3}$$

Equation of state of the fluid and reservoir compressibility:

Fluid compressibility: $$c_w = \frac{1}{p}\frac{\partial p}{\partial p}$$

Rock compressibility: $$c_r = \frac{1}{1-\varphi}\frac{\partial \varphi}{\partial p} \tag{4}$$

Total compressibility: $$c_t = \varphi c_w + (1-\varphi)c_r$$

Combining the equations above results in the pressure diffusion equation, giving:

$$\frac{\partial^2 p}{\partial r^2} + \frac{1}{r}\frac{\partial p}{\partial r} = \frac{\mu c_t}{k_r}\frac{\partial p}{\partial t} = \frac{S}{T}\frac{\partial p}{\partial t} \tag{5}$$

where $T = \frac{kh}{\mu}$ = The transmissivity
s = Storativity;
h = Effective reservoir thickness;
k = Permeability of the rock matrix;
μ = Dynamic viscosity of the fluid.

Transmissivity *T* describes the ability of the reservoir to transmit fluid, largely affecting the pressure gradient between the well and the reservoir; thus, it governs how fast fluids can flow to the well. Storativity *S* defines the volume of fluid stored in the reservoir, per unit area, per unit increase in pressure and has great impact on how fast the pressure wave can travel within the reservoir.

The *Theis solution* (line source solution), an integral solution for the above pressure diffusion equation (Earlougher, 1977; Horne 1995; Jónsson, 2011) is obtained with assumptions that the reservoir is infinite, and the radius of the wellbore is negligible, and setting the initial and boundary conditions as follows:

Initial condition: $p(r,0) = p_i$ for all $r > 0$

Boundary conditions:

At infinity: $\lim_{r\to\infty} p(r,t) = p_i$ for all $t > 0$

At the well: $Q = \frac{2\pi kh}{\mu} \lim_{r\to\infty} \left[r \frac{\partial p}{\partial r} \right]$ for all t >0

The solution to the radial pressure diffusion equation, $p(r,t)$, for the above initial time and boundary conditions is then:

$$p(r,t) = p_i + \frac{q\mu}{4\pi kh} E_i \left[-\frac{\mu c_t r^2}{4kt} \right] \tag{6}$$

E_i is the exponential integral defined as:

$$E_i(-x) = -\int_x^\infty \left(\frac{e^{-u}}{u} \right) du \quad with\ x = \frac{\mu c_t r^2}{4kt} \tag{7}$$

For small values of $x = \frac{Sr^2}{4\pi T}$, i.e. $x < 0.01$ we can use:

$$E_i(-x) \approx -\ln(x) - \gamma$$

where $\gamma = 0.5772$ is the Euler's constant.

Therefore, if t > 100 $\mu c_t r^2/4kt$ and if ln$x$ = 2.303 log$x$, then the solution for the radial pressure diffusion equation can be simplified to:

$$p(r,t) = p_i + \frac{2.303q\mu}{4\pi kh} \left[log\left(\frac{\mu c_t r^2}{4kt} \right) + \frac{\gamma}{2.303} \right] \tag{8}$$

The computer program WellTester (Júlíusson et al., 2010) was used in the analysis of the injection test data to estimate geothermal reservoir properties in the vicinity of the well. It has mathematical models inbuilt so after observed data is input, a specific model is chosen. Then the reservoir properties that this model relies on are calibrated until a good fit is seen between the actual observation and the theoretical pressure transient results obtained from the model. Models are based on the pressure diffusion equation.

4.1.2 Testing of wells

An injection test was conducted in four steps but first by positioning the pressure tool just below the perceived feed zone and pumping water into the well. The pumping rates and duration were 16.7 kg/s for 4 hrs, 21.7 kg/s for 3 hrs, 26.7 kg/s for 3 hrs, and 31.7 kg/s for another 3 hours. The model that best fitted the data was: Homogenous reservoir, constant pressure boundary, and constant skin and wellbore storage.

Injection testing is used to determine the gross productivity of a well immediately after drilling is completed. Injectivity testing provides an estimate on the wells' performance and the choice of equipment to be used in subsequent tests will be known. An injectivity index (II) is defined as the ratio of the injection flow (ΔQ) divided by the change in the stabilized reservoir pressure (ΔP). Pressure can be monitored at the pumps or downhole by positioning the tool stationary at a depth while injection is carried out.

$$II = (\Delta Q/\Delta P)$$

Consider higher permeability wells that have inflow at upper levels during injection. Since the well bore pressure during injection is lower than the formation pressure at higher elevations, the pressure distribution is the hydrostatic pressure of the injected cold water. Then the value of the gross permeability may not be representative of the formation. If the tool is located further down the well, the comparison of downhole pressure changes with the surface injection rate will be erroneous. Injectivities are obtained from the pressure build-up recorded down hole by the tool, as shown in the plot in Figure 18. If the injection rate is varied with time the stable pressure achieved at each stage are used with injection rate to calculate the injectivity. Results are tabulated in Table 2. Well OW 905A posted the highest injectivity rate of 3.99 (L/s)/bar, OW 916A followed with 2.89 (L/s)/bar and OW 913A had the least injectivity rate of 1.12 (L/s)/bar. Injection test data for OW 907A were not available.

TABLE 2: Injectivity index for wells OW 905A, OW 913A, and OW 916A

Well	Injectivity ((L/s)/bar)
OW 905A	3.99
OW 913A	1.12
OW 916A	2.89

OW 913A: The pressure tool was stationed at 2500 m depth in this well. Figure 18 shows the well's pressure build up. Only the step with data that fit best in the model is considered and the estimated parameters are tabulated in Table 3. Figure 19 plots the model response and the raw data corresponding to step 3 which fit best the model.

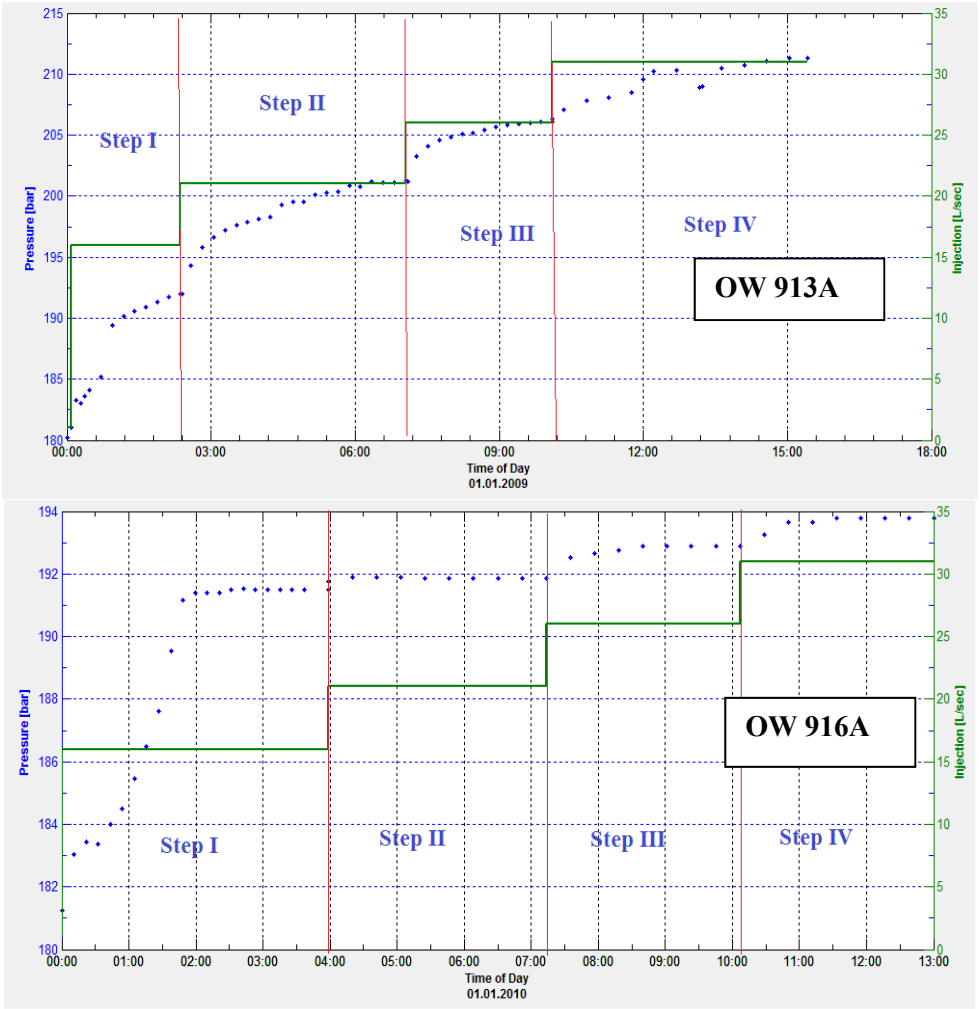

FIGURE 18: Injection tests for wells OW 913A (above) and OW 916A (below); injection rate (L/s) and pressure build up (bar)

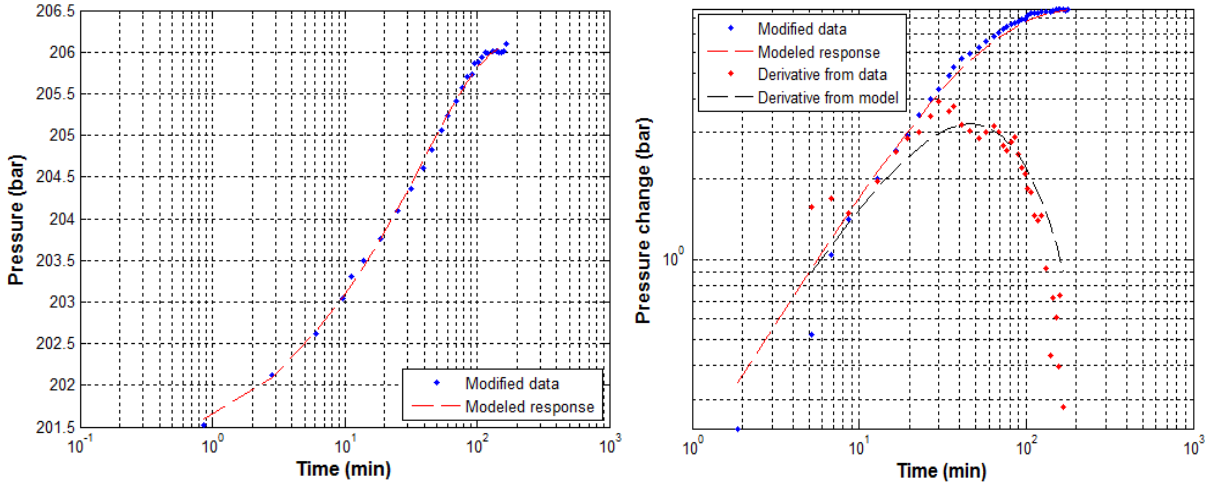

FIGURE 19: Well OW 913A, fit between model and selected data on a log-linear scale (left) and on a log-log scale (right) for step 3

OW 916A: The pressure tool was stationed at 2550 m depth in this well and Figure 18 shows the pressure build up as recorded. Data in step 4 fitted best with the model therefore and was only considered and the estimated parameters are tabulated in Table 3. Figure 20 shows a plot of the modelled response with the raw data for step 4 from well OW 916A.

TABLE 3: Summary of the reservoir parameters obtained from the injection data in wells OW 913A and OW 916A

Well	Transmissivity (m^3/Pa.s)	Storativity (m^3/Pa.m^2)	Skin factor	Permeability (mD)
OW 913A	3.60×10^{-8}	2.06×10^{-8}	-0.18	3.43
OW 916A	4.77×10^{-8}	4.01×10^{-8}	-0.18	2.26

Transmissivity values obtained were on the order of 10^{-8} m^3/Pas and were within the range obtained before from the wells in the Domes field (Kariuki, 2003; Mwarania, 2010). Storativity is also on the same order as estimated by Mwarania (2010). The permeability obtained is in the range of 2.26 to 3.43 mD.

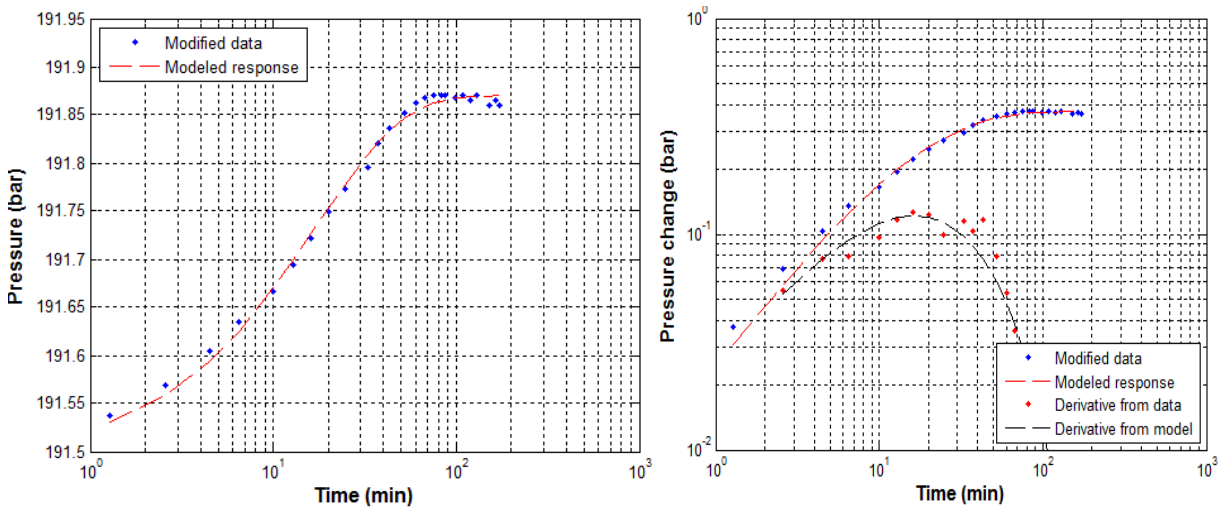

FIGURE 20: Well OW 916A, fit between model and selected data on a log-linear scale (left) and on a log-log scale (right) for step 4

4.2 Production tests

To further characterize the reservoir, once a well has heated up and recovered in temperature and pressure, it is discharged. The well is opened up and allowed to flow to the atmosphere. If the well cannot initiate self-discharge, it is stimulated by pressurizing with air. Geothermal high-temperature wells are usually discharged into a silencer which also acts as a steam-water separator at atmospheric pressure. The two-phase mixture is flowed through different sizes of lip-pressure pipes into the silencer which effectively varies the wellhead pressure. Production in terms of wellhead pressure and the flow rate can be obtained. The steam from the separator disappears up into the air but the liquid water is measured as it flows from the silencer over a V-notch weir. The following flow parameters are then measured:

- Wellhead pressure (WHP)
- Lip pressure (Pc)
- Height of water in the V-notch weir.

Using the James lip-pressure method (Equation 9), the output parameters from the discharging well are calculated (Grant et al., 1982) by:

$$Q = 1{,}835{,}00\ A\ \frac{P_c^{0.96}}{H^{1.102}} \tag{9}$$

where Q = Total mass flow rate (kg/s);
A = Cross-sectional area of the lip pipe (m^2);
P_c = Critical pressure at the end of the lip pipe (bar-a);
H = Fluid enthalpy (kJ/kg).

The total mass flow rate obtained from this method can be related to the water flow rate measured at the V-notch weir after separation in the silencer:

$$Q_t = Q_w \frac{H_s - H_w}{H_s - H_t} \tag{10}$$

Since the well is being discharged into the atmosphere, the specific enthalpies of steam and water at atmospheric conditions, H_s = 2676 kJ/kg and H_w = 419 kJ/kg are substituted in Equation 10; it then reduces to:

$$Q_t = Q_w \frac{2256}{2676 - H_t} \tag{11}$$

Equations 9 and 11 are then combined and solved for H_t , the total fluid enthalpy, which gives:

$$1{,}835{,}00\ A\ \frac{P_c^{0.96}}{H^{1.102}} = Q_w \frac{2256}{2676 - H_t} \tag{12}$$

From Equation 11 the total enthalpy H_t is obtained and used in calculating the following parameters:

- Total mass flowrate – from Equation 11; once the total enthalpy (H_t) is obtained along with measured weir flow (Q_w), the total flowrate can be calculated, and also
- Water flowrate;
- Steam flowrate;
- Flow enthalpy; and consequently,
- Electrical power.

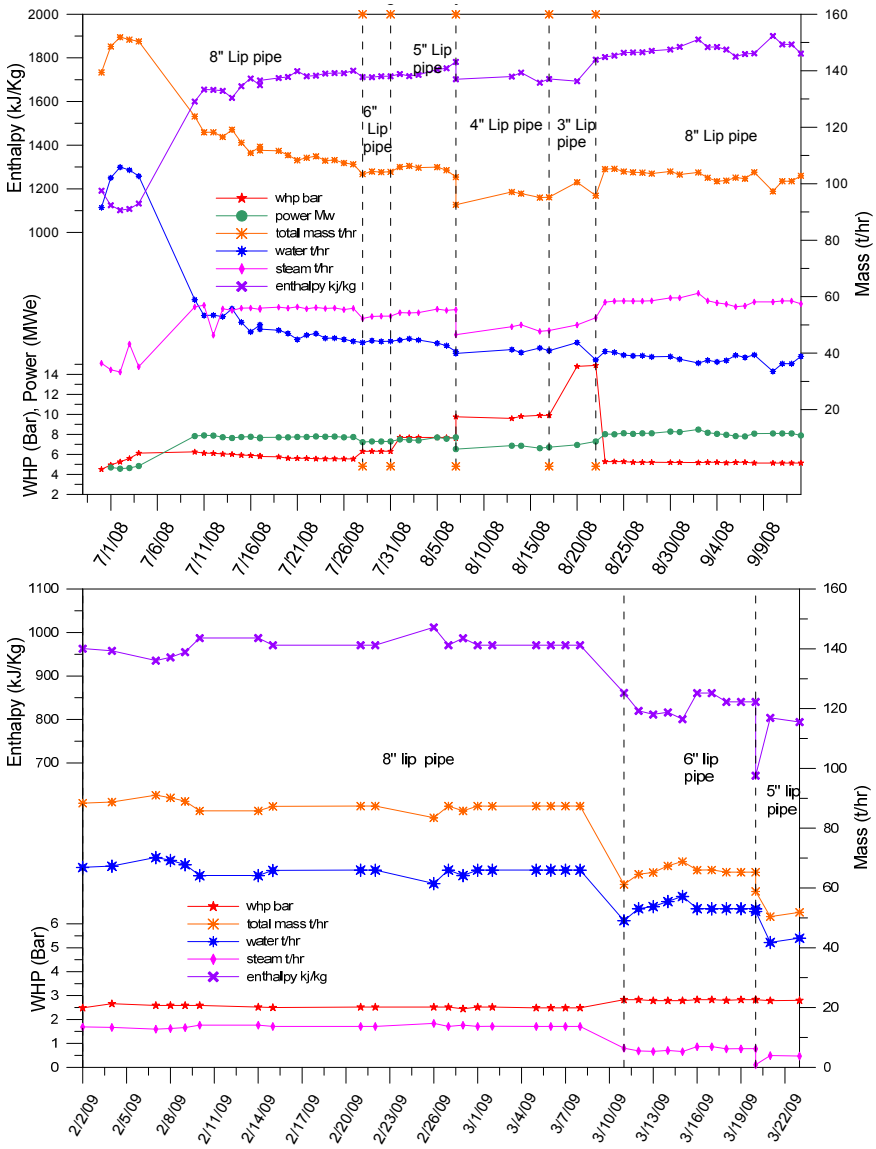

FIGURE 21: Discharge history of wells OW 907A (above) and OW 905A (below)

OW 907A was tested with five lip pipes (3, 4, 5, 6 and 8"). The well sustained discharge on all five lip pipes. Discharge history for OW 907A (Figure 21): the well initially had a high total mass flow in which the water flow was high. With time the water flow dropped, steam flow increased and total mass reduced, accompanied by an increase in enthalpy. The well stabilized for all applied wellhead pressures. Table 4 shows the average output summary for this well.

OW 905A sustained discharge on only three pipes used. Of the total mass flow, the water phase dominated the steam phase. Pressures recorded were less than 3 bars. The well stabilized with the applied wellhead pressures. Enthalpy declined with a decline in mass flow as seen in Figure 21. Table 5 shows the output summary.

TABLE 4: Output summary for well OW 907A

Lip pipe	Whp (bar-a)	Mass (t/hr)	Steam (t/hr)	Enthalpy (kJ/kg)
8"	5.57	108.34	55.89	1728.15
6"	6.31	104.04	52.88	1713.97
5"	7.66	103.98	55.40	1764.55
4"	9.83	95.88	48.74	1708.53
3"	14.90	95.79	52.56	1792.25

TABLE 5: Output summary for well OW 905A

Lip pipe	WHP (bar-a)	Mass (t/hr)	Steam (t/hr)	Enthalpy (kJ/kg)
8"	2.54	88.04	13.55	964.98
6"	2.82	65.52	6.06	835.34
5"	2.81	53.73	2.86	756.37

OW 913A could not self-discharge. There were several attempts made to initiate discharge by pressurizing with air but there was no success. The well was given more time to recover and was later able to initiate self-discharge. The well was discharged on 4", 5", 6" and 8" lip pipes (Figure 22), but could not sustain discharge on a 3" lip pipe. The well achieved stable discharge for the applied wellhead pressures. Table 6 shows an average output summary for this well. It is noted that the well recorded pressures lower than 5 bars while discharging on the 6" and 8" lip pipes.

OW 916A was discharge tested with five lip pipes (3, 4, 5, 6" and 8") and it sustained discharge as shown in the discharge history for OW 916A in Figure 22. The well initially had high total mass flow in which the water flow was high. With time, the water flow dropped, steam flow increased and the total mass reduced but enthalpy increased. Table 7 shows an average output summary for this well.

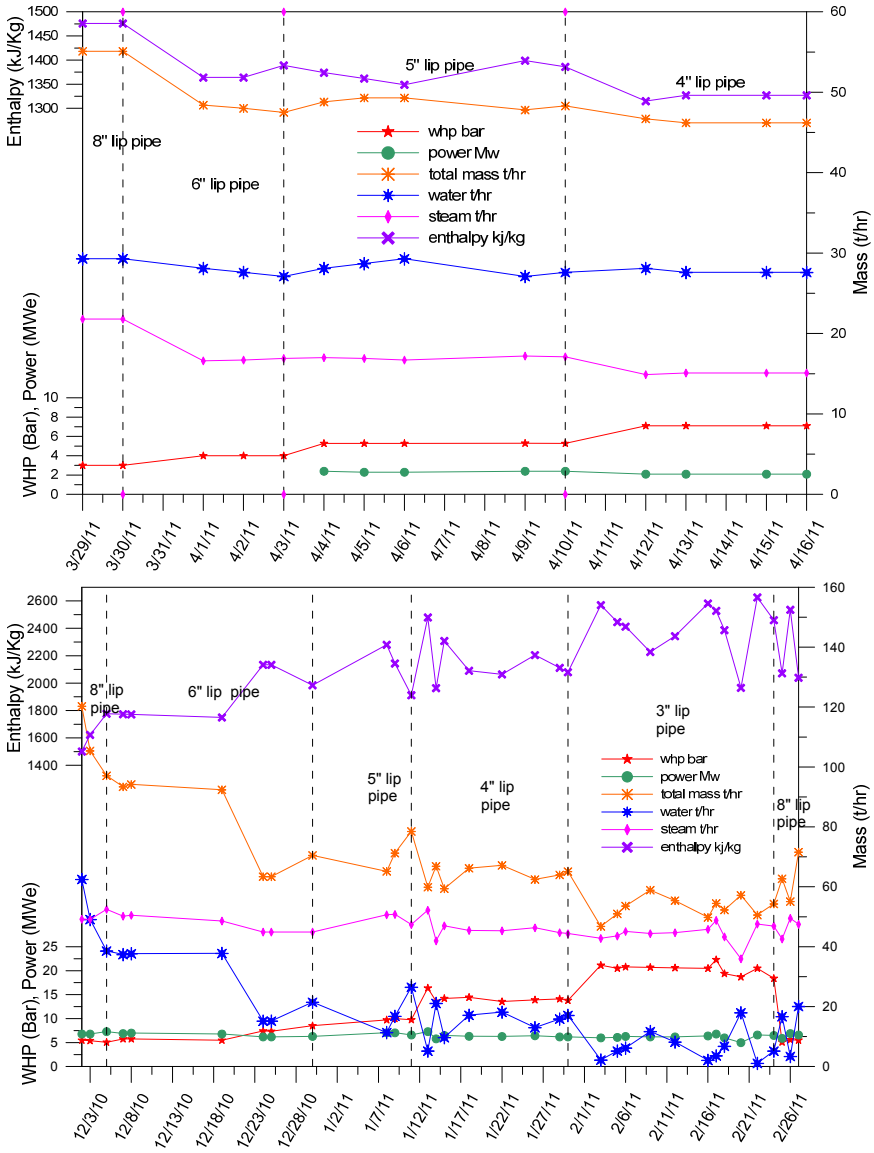

FIGURE 22: Discharge history of well OW 913A (above) and OW 916A (below)

In the interpretation of production tests carried out in a well, output parameter variations are plotted with stable wellhead pressure prevailing when observation are made. Parameters monitored are mass flow and enthalpy depending on the reservoir under testing. A plot of total mass flow rate with wellhead pressure is the characteristic, or output curve. In designing and operating a geothermal power plant, output curves are important as they give the amount of steam and brine available from a well at a given throttle condition, i.e. pressures at which the plant is to be run.

TABLE 6: Output summary for OW 913A

Lip pipe	Whp (bar-a)	Mass (t/hr)	Steam (t/hr)	Enthalpy (kJ/kg)
8"	3.00	55.10	21.80	1476
6"	4.00	47.50	16.90	1389
5"	5.28	48.70	16.98	1374
4"	7.10	46.20	15.10	1327

TABLE 7: Output summary for OW 916A

Lip pipe	Whp (bar-a)	Mass (t/hr)	Steam (t/hr)	Enthalpy (kJ/kg)
8"	5.32	107.60	50.27	1633.53
6"	6.67	79.81	47.40	1922.88
5"	9.83	71.65	49.63	2112.17
4"	14.25	63.90	45.93	2162.97
3"	20.32	53.13	44.45	2413.56

In the characteristic curves (Figure 23) for the four wells, it was observed that OW 907A gave the highest mass flow followed by OW 916A; the least flow was in OW 913. All the wells had declining mass flow with increasing wellhead pressure. OW 913 had the least mass and lowest pressures. Mass flows in well 905A declined rapidly with a slight rise in pressure, indicating that the well has single-phase water feeds (Grant et al., 1982).

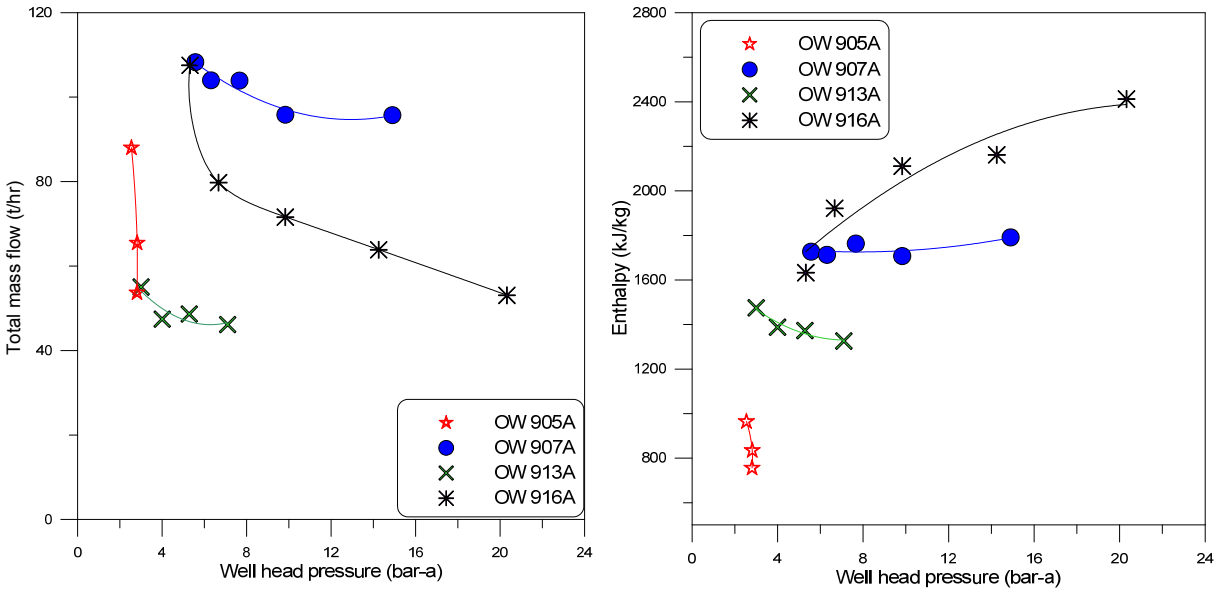

FIGURE 23: Output curves for wells OW 905A, OW 907A, OW 913A and OW 916A; total mass flow vs. wellhead pressure (left) and enthalpy vs. wellhead pressure (right)

The enthalpy curves are also shown in Figure 23. OW 916A showed increasing enthalpy with reducing flows, suggesting two phase conditions in the reservoir. Throttling the well raised the pressures and, due to the relative permeability, steam with higher enthalpy was the mobile phase. Whereas for well OW 913A, there was a decrease in enthalpy with the decrease in mass flow, a characteristic of a two-phase reservoir with lower permeability. Enthalpy at small flow rate, i.e. high WHP, is close to liquid water, while at high flow rates (low WHP) enthalpy is higher due to flashing associated with drawdown; the increase in flowing enthalpy with decreasing wellhead pressure is due to boiling in the formation. As for well OW 907A, the relatively stable enthalpy suggests a reservoir with high permeability and, with fluid entering the well at all flow rates of a steam-water mixture, enthalpy above the reservoir water. As for well 905A, the decline in enthalpy with a decline in mass flow confirms that the well is in the periphery with a liquid-dominated feed zone; thus, the enthalpy is close to the saturated liquid.

5. CONCEPTUAL MODEL

Domes field is bound on the west by the Ol njorowa gorge, and the ring of domes both to the east and to the south. Geothermal manisfestations are strongly related to the geologic structures; fumerals are concentrated along the ring structure on the eastern side of the field and along the N-S trending fault (Clarke et al., 1990; Mungania, 1992). The main recharge paths are NNW-SSE and NW-SE east-dipping major rift faults exposed on the Mau escarpment. N-S rift-floor faults and fractures control axial shallow groundwater flow through the geothermal system and the major rift-forming faults provide deep recharge. The Gorge farm fault, an ENE-WSW trending fault, is the most important permeability structure. Dyke swarms exposed in the Ol'Njorowa gorge trend in a north-northeast direction, indicating recent reactivation of faults with that trend. Recharge to the Domes reservoir is located in the north where the NW-SE fault intersects N-S and NE-SW faults (Gorge farm fault). Omenda (1998) noted that wells are more likely to show similar reservoir characteristics in a general N-S direction that coincides with rift-floor fault patterns; he also noted that predicting the permeability distribution in the field without drilling a well would be difficult. The contrasting productivity of wells drilled from the same pad but in different directions (OW 916 and OW 916A, and OW 904 and 904B) reinforces this fact. Wells drilled close to exposed N-S faults have a characteristic inversion (e.g. OW 905A), evidence of the influence that shallow structures have on reservoir characteristics.

Results of geophysical resistivity measurements, when compared with alteration minerals and measured temperature data in a section connecting wells 901, 902, 903, 904, 908A, 909 and 910, compares well except in well 901 and partly 904 where measured temperature was not in equilibrium with alteration mineralogy since heating had occurred (Lichoro, 2009). Contrarily, it was noted in the southwest of Domes field where the alteration minerals are relicts in OW 902 and where cooling had occurred (Lagat, 2004). High-temperature alteration minerals were sampled in well OW 902; the measured temperatures were lower.

A fault oriented NNE-SSW passing through OW 903 is channelling shallow environmentally contaminated groundwater into the well. Nitrogen gas concentrations from the well's fluid discharge have a maximum value when compared to other wells in Greater Olkaria geothermal area (GOGA) (Karingithi, 2002). Wells intercepted by this fault have distorted temperatures at an elevation of 1000 m a.s.l. Figure 24 shows the horizontal temperature distribution at different elevations. At an elevation of 1000 m a.s.l., the effects of the NNE-SSW fracture on the temperature distribution can be seen. In the same figure the temperature distribution at sea level can be seen to the north around OW 905A; the cold temperatures observed can be attributed to recharge to the system. Solute and gas geothermometry indicate high temperatures in the range of 250-350°C in the Domes reservoir, which is in agreement with the temperatures observed in the cross-sections.

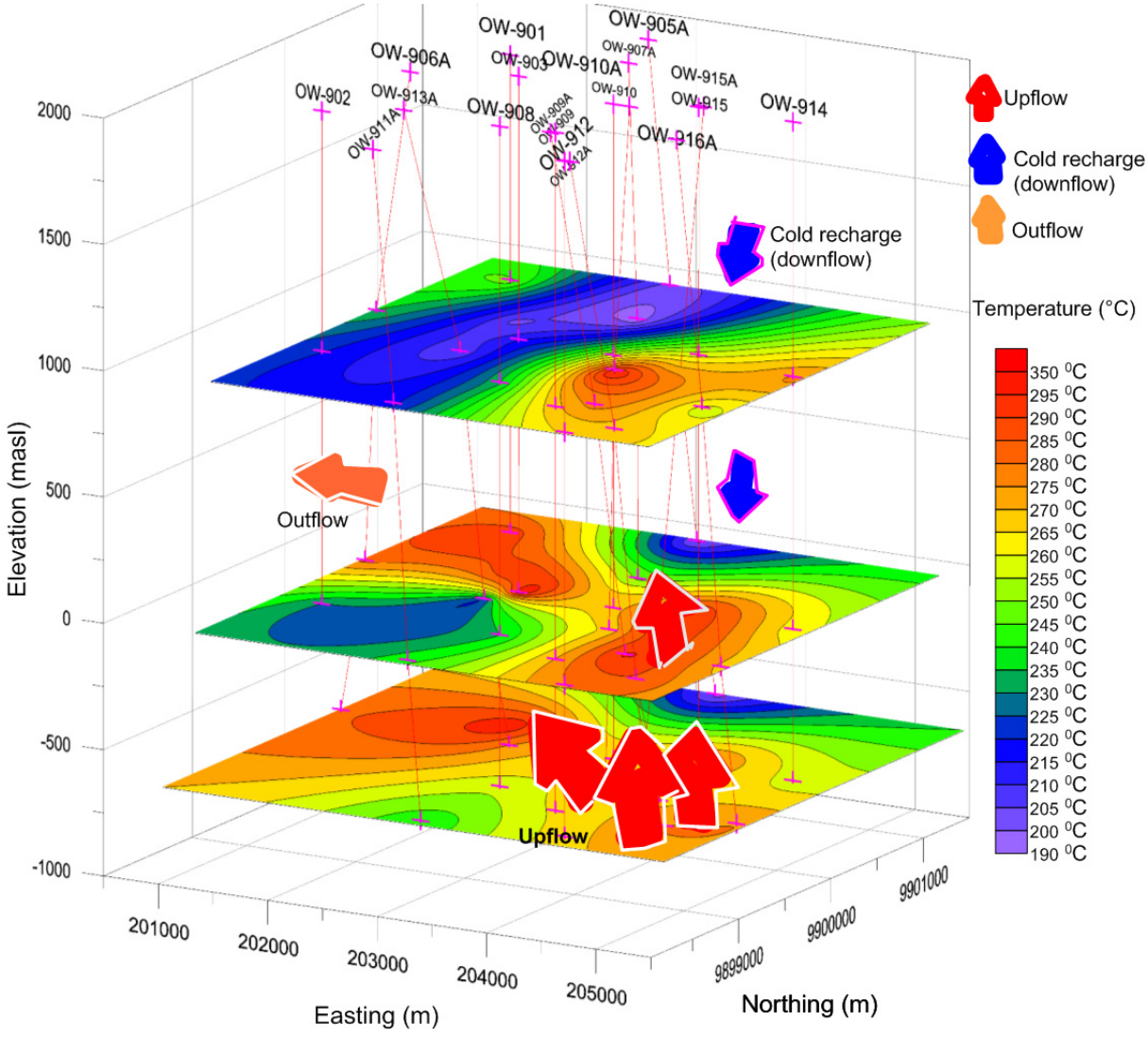

FIGURE 24: Conceptual model showing horizontal distribution of temperature (°C) at different elevations with locations of upflows, recharge and outflow

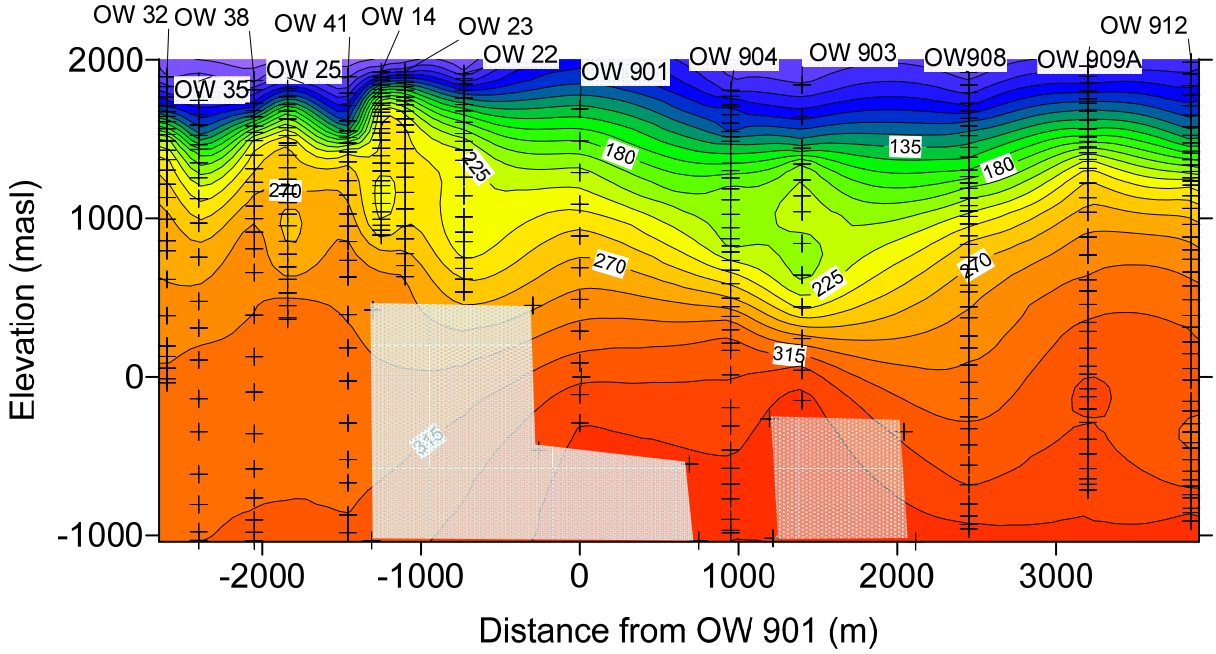

FIGURE 25: A NNW-SSE trending vertical cross-section for temperature for the Olkaria East and Domes wells

In Figure 25, a cross-section extending from the southeast of Domes to Olkaria East field is shown. The temperatures show convection to the extreme ends of the cross-section from OW 32 - OW 23 in Olkaria east and to OW 908 - OW 912 in Domes. A conductive temperature distribution was noted in OW 901 from the surface where the temperature contours were equi-spaced with depth. OW 903 has convection from 1500 to 500 m a.s.l. from where the isolines are equi-spaced with depth. The wells have varying depths and the masked area is where data may not be conclusive as the wells there are shallow.

Also in Figure 17 (Section 3.2), a plume is seen from OW 908 peaking in OW 909A and extending to OW 916A, as the data constraint is only to OW 916A. Upflow could be extending beyond OW 916A.

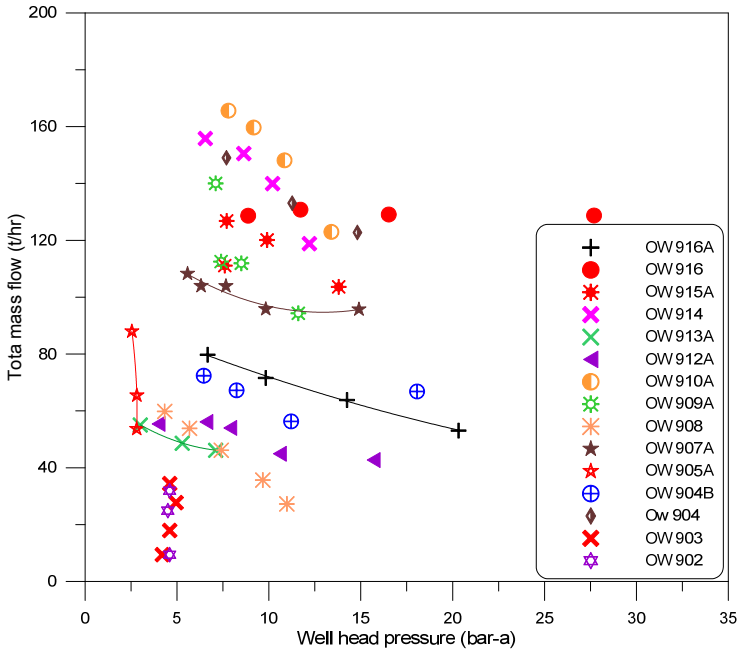

FIGURE 26: Output curves for Olkaria Domes wells, total mass flow vs. wellhead pressure

The same case applies to constraints in OW 912A. As discussed in Section 3.2, the upflow is located to the east and southeast of Domes field in the area around OW 909, OW 910, and OW 915, including OW 916 and beyond. The mentioned wells follow, or closely follow, the BPD curve, a characteristic of wells in an upflow area.

In Figure 26, wells from the Domes are compared and, within the proposed upflow, have higher total mass flow. The wells in the same area that have low flows maintain the same flow even at high wellhead pressures, indicating that there is good pressure support. The small flow is attributed to the permeability and reservoir structural effects. Wells on

the eastern side of Domes field also have high enthalpy in the tested wells; the range is 2250-2500 kJ/kg. Wells on the western side have low enthalpy, with OW 902 registering 1100 kJ/kg. Wells on the western part of the field that have high flows such as OW 904 (Figure 25) which had an enthalpy of 1233 kJ/kg, which is lower than that of wells in the upflow area.

6. VOLUMETRIC ESTIMATION OF RESERVOIR CAPACITY

This method involves the calculation of the heat present in the reservoir rocks and in the fluid entrapped in the formation by integrating the heat capacity and the temperature over the volume of the geothermal system. As discussed by Halldórsdóttir et al. (2010), assumptions are made that the heat capacity and temperature are homogeneous in horizontal directions and that they vary only in the vertical direction; also, for simplicity, the geothermal system is often divided into different layers where the heat capacity is constant in each layer and depends only on the specific heat and density of the rock and water. As only a small portion of the total heat in the system is recoverable, a recovery factor, R, which is a ratio of recoverable heat from the total heat in the system, is introduced. The recoverable heat is then converted into electrical energy using conversion efficiencies:

Electric energy:
$$Q_e = \eta_e RAC \int_{z_0}^{z_1} \lfloor T(z) - T_0 \rfloor \, dz \tag{12}$$

Electric power:
$$P = \frac{Q_e}{t} \tag{13}$$

where C is the heat capacity per volume; $C = C_w \rho_w \varphi + C_r \rho_r (1 - \varphi)$, R is the recovery factor, φ is the porosity of the rock, C_r is the specific heat of the rock and ρ_r is the density of the rock, C_w is the specific heat of the water and ρ_w is the density of the water. A is the surface area of the geothermal system, $T(z)$ is the reservoir temperature and T_0 is the reference temperature, in this case the cut-off temperature, and t is the production time of the electric power in seconds.

There are uncertainties in the parameters used in volumetric calculations; reservoir properties such as porosity lie within a certain range rather than having one fixed value. This is also the case with the other parameters used to determine the energy reserve. This uncertainty is addressed using Monte Carlo calculations where a probability distribution is defined for parameters.

From the interpretation of logs during warm-up of the wells, the obtained temperature closely follows the boiling point with depth (BPD) curve. The relationship of the boiling point with depth by James (1970) was used to assign a distribution for the reservoir temperature:

Reservoir temperature:
$$T(z) = X \, . \, 69.56(z - Z_\delta)^{0.2085} \tag{14}$$

where X is a ratio factor describing the deviation from the true boiling curve that runs from zero to one, z_δ, is the translation in z direction in order to meet the upper boundary conditions, and $T(z_0)$ at z_0.

Table 8 shows the parameters used in volumetric reservoir estimation with Monte Carlo analysis. Parameters were assigned different distributions. According to the probability distribution, it is most probable with a 6% probability that the electrical power production capacity lies between 280 MWe and 305 MWe if the recoverable heat is used for 50 years. Also from the statistics of the distribution, the volumetric model predicts with 90% confidence that power production capacity lies between 170-425 MWe for 50 years. From the statistics of the cumulative probability, the volumetric model predicts with 90% probability that at least 210 MWe can be produced for a production period of 50 years. The above is summarized in Table 9.

TABLE 8: Parameters in Monte Carlo analysis for the Olkaria Domes geothermal field

Description	Variable	Distribution type	Minimum value	Most probable value	Maximum value
Surface area	A	Triangular dist.	23 km^2	27 km^2	36 km^2
Upper depth	$Zmin$	Constant	N/A	0 m	N/A
Lower depth	$Zmax$	Constant	N/A	3000 m	N/A
Porosity	φ	Constant dist.	8%	N/A	10%
Specific heat of rock	CR	Constant dist.	900 J/(kg°C)	N/A	980 J/(kg°C)
Density of rock	ρ_R	Constant dist.	2600 kg/m3	N/A	2900 kg/m3
Specific heat of water	CW	Constant	N/A	5200 J/(kg°C)	N/A
Density of water	ρ_w	Constant dist.	700 kg/m3	N/A	800 kg/m3
Recovery factor	R	Triangular dist.	10%	20%	25%
Cut-off temperature	T_0	Constant	N/A	170°C	N/A
Electric conversion coeff.	η_e	Constant	N/A	12%	N/A
Production time	t	Constant	N/A	50 years	N/A
Boiling curve ratio	x	Triangular dist.	75%	90%	100%

TABLE 9: Statistical parameters for the probability distribution for electric power production for the Olkaria Domes geothermal field estimated by the Monte Carlo method for a production period of 50 years

Statistical sizes	Values (MWe)
Most probable value (6% probability)	280-305
90% confidence interval	170-425
Mean	290
Median	290
Standard deviation	73
90% limit	210

7. SIMPLE NUMERICAL MODEL

The analysis in the preceding chapters provides the background for the development of the simple numerical model that characterizes the Domes reservoir in its natural state which will, in turn, provide the benchmark, pre-exploitation natural state of the field. Exploitation of the field distorts the flow pattern established in the natural convecting system. The numerical model will then be calibrated against the measured field data. The conceptual model developed was tested against the natural thermodynamic conditions of the field to obtain a match with the spatial distribution of temperatures and pressures.

The model was developed using the TOUGH2/ iTOUGH2 (Finsterle, 1993; Pruess et al., 1999) computer codes. Grid geometry in Figure 27 shows the layout of a grid covering wells in Olkaria Domes field. The model covers an area of about 27 km^2 and is partitioned into 31 grid blocks. Vertically, the model has a small surface layer at atmospheric conditions, followed by an impermeable cap rock 700 m thick, beneath which underlies a permeable reservoir of 2300 m (Figure 28) that is further partitioned into seven layers giving a total of 279 grid blocks.

Boundary conditions were: top and bottom layers were set inactive. The sinks and sources are located in the second and eighth layer, respectively (B and H). Dominant fractures were as indicated in Figure 27 and upwelling fluids flow along these fractures.

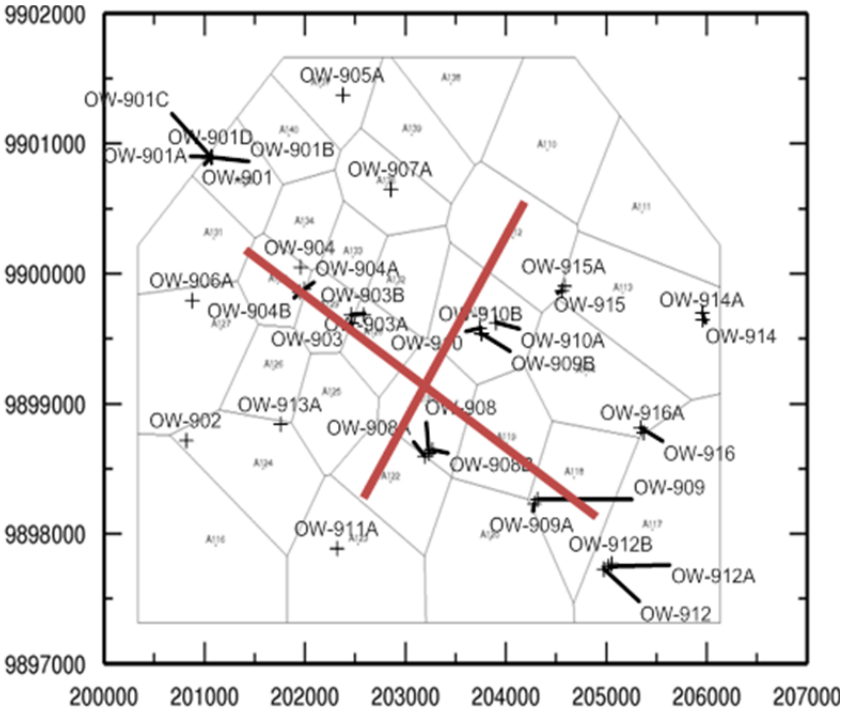

FIGURE 27: The horizontal grid of the model, also showing dominant fractures (heavy red) and well locations

The natural state simulation run was done for 10,000 years until a steady state situation, agreeing closely with the measured temperatures and pressure values in most parts of the field, was found. Inverse modelling was used to assist the manual calibration process where rock parameters and boundary conditions were changed. Other parameters adjusted were: strength of the upflow (both enthalpy and upflow rate), vertical and horizontal permeabilities, and the strength of outflow and steam losses. The results of reservoir temperature at almost steady state conditions were compared with the estimated formation temperatures and initial pressures for the wells.

The results of the simulation are shown in Figure 29 for the selected wells. Graphs, of temperatures obtained at almost steady state conditions of the reservoir over geological time from when the geothermal system developed, were compared to the interpreted formation temperatures. The model gave a good overall match to the estimated reservoir temperatures and is representative of the quality of a match obtained from most of the available field data. Table 10 shows the flow rates and enthalpies representing the natural state model.

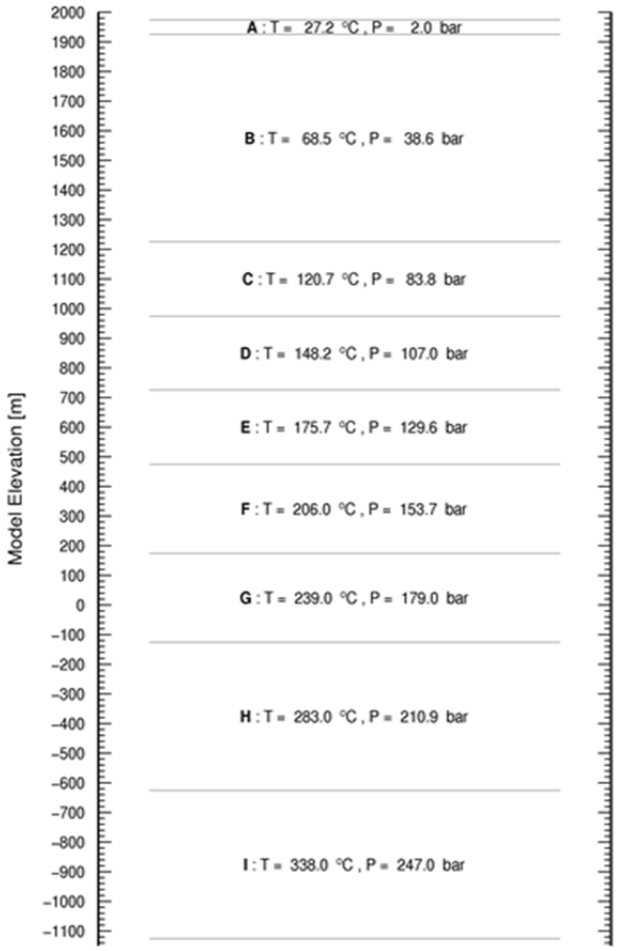

FIGURE 28: The vertical grid of the model

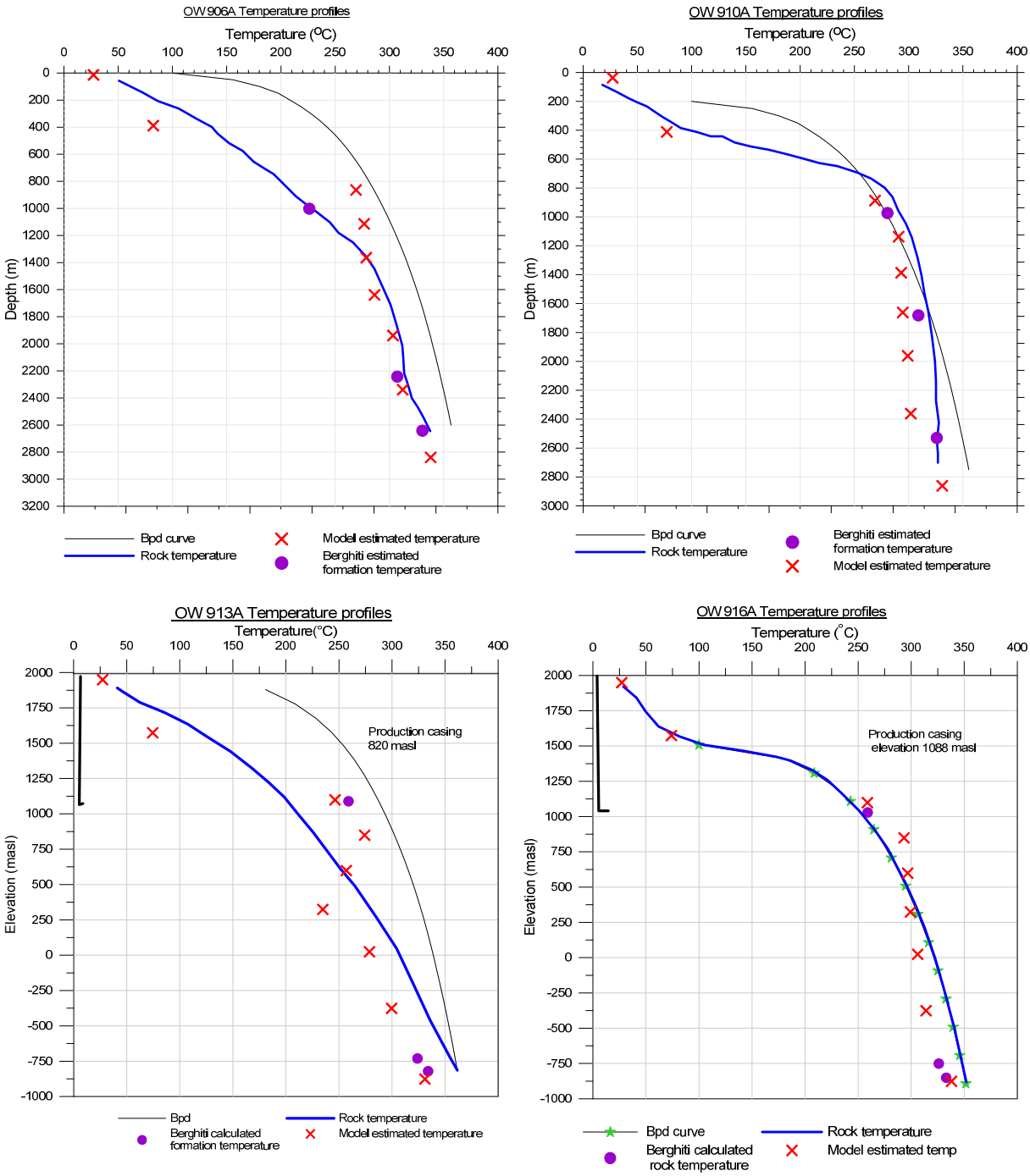

FIGURE 29: Comparison of formation temperature and model calculations for downhole temperatures of wells 906A, 910A, 913A and 916A

TABLE 10: Enthalpy and flow rates for sources and sinks in the Olkaria model

	Element	Mass (kg/s)	Enthalpy (kJ/kg)
Source	HA114	9.0	1600
	HA115	8.5	1600
	HA119	7.0	1600
Sink	BA116	3.0×10^{-10}	500
	BA127	3.0×10^{-10}	500

8. DISCUSSION AND CONCLUSIONS

Olkaria Domes geothermal field can be classified as a high-temperature field in two-phase conditions. From the estimated formation temperatures, the wells to the east and southeast in Domes field follow the boiling point depth curve; temperatures of more than 300°C were recorded. The upflow is located in the east and southeast parts of Domes around wells OW 909, OW 910, OW 915, including OW 916 and probably extending eastwards to the caldera rim (ring structure). Recharge to the field is to the north; pressure potential fluid flow runs from the north to the south and southwest of the field. Well OW 902 discharged at low pressures, and had low mass flow rates with low enthalpy close to saturated water, while the wells on the eastern side discharged high enthalpies and high flow rates, indicating good pressure support to the eastern part and low pressure to the southwest part of the field.

The natural state model was obtained as a steady state condition of simulation of geothermal field development over a geological period of 10,000 years. The model gave a good overall match to the estimated reservoir temperature and is representative of the quality of a match obtained from most of the available field data. Production in the field has not started and all the data available represent natural state; thus, the simple 3-D natural state model developed has provided a benchmark (pre-production) reference for future calibrations after production. The model developed has few grids blocks and improvements can be made by refining the grid size for refinement and recalibration of the geological structure. The model could be further calibrated to match the enthalpy data from the wells.

Geo-scientific information indicates that the subsurface main recharge paths are NNW-SSE and NW-SE east-dipping major rift faults exposed on the Mau escarpment. N-S rift-floor faults and fractures control axial shallow groundwater flow through the geothermal system, and the major rift-forming faults provide deep recharge. The Gorge farm fault, an ENE-WSW trending fault, is the most important permeable structure. Dyke swarms, trending in a north-northeasterly direction, enhance the permeability in the field. Recharge to the Domes reservoir is located to the north where the NW-SE fault intersects N-S and NE-SW faults.

Well test analysis gave a reservoir transmissivity range of between 3.6 and 4.8×10^{-8} m^3/Pa.s, and an effective permeability range of 2.3-3.4 mD with analysed wells OW 913A and OW 916A. Data for well OW 907A were not available; data for OW 905A was scattered and could not be used in the derivative analytical model used in the well tests.

Volumetric reservoir estimates show that Olkaria Domes geothermal field can support more than 210 MWe for a period of 50 years with 90% confidence.

ACKNOWLEDGEMENTS

I would like to express my gratitude to Dr. Ingvar B. Fridleifsson, the Director of the UNU Geothermal Training Programme for the chance to take part in the Programme, and to the Deputy Director, Lúdvík S. Georgsson for his help and support. My appreciation also goes to Ms. Thórhildur Ísberg, Mr. Ingimar G. Haraldsson, Mr. Markús A.G. Wilde and Ms. Dorthe H. Holme for their great assistance during my study and stay in Iceland. Thanks to the entire staff of UNU, Orkustofnun and ÍSOR. My sincere appreciation and thanks to my supervisors, Ms. Saeunn Halldórsdóttir, Ms. Sigrídur Sif Gylfadóttir, both from ISOR, and Mr. Andri Arnaldsson from Vatnaskil Consulting Engineers, for their tireless assistance and advice during my research project.

I am grateful to my employer, the Kenya Electricity Generating Company Ltd. – KenGen, for the opportunity to attend the training and for providing the information used in this work. To the UNU fellows I say, thank you very much for the wonderful time and discussions that we shared together.

To my colleagues in reservoir engineering, Mr. Urbanus Mbithi, Mr. Felix Mwarania and the team, thank you so much for ensuring I got the data.

Thanks to my parents, Mr. and Mrs. R.K. Koskey, for their love, support and encouragement. Finally, thanks to God for his grace.

REFERENCES

Arason, Th., Björnsson, G., Axelsson, G., Bjarnason, J.Ö., and Helgason, P., 2003: *The geothermal reservoir engineering software package Icebox, user´s manual.* Orkustofnun, Reykjavík, manual, 53 pp.

Baker, B.H., 1987: Outline of the petrology of the Kenya rift alkaline province. In: Fitton, J.G., and Upton, B.G.J. (eds.), *Alkaline igneous rocks*. Geol. Soc. Spec. publ., 30, 293-311.

Clarke, M.C.G., Woodhall, D.G., Allen, D., and Darling G., 1990: *Geological, volcanological and hydrogeological controls on the occurrence of geothermal activity in the area surrounding Lake Naivasha, Kenya, with coloured 1:100 000 geological maps.* Ministry of Energy, Nairobi, 138 pp.

Earlougher, R.C., 1977: *Advances in well test analysis*. Soc. Petr. Eng., Monograph 5, 264 pp.

Finsterle, S., 1993: *iTOUGH2, user's guide, version 2.2*. Lawerence Berkeley Laboratory, University of California, 137 pp.

Giggenbach, W.F., 1991: Chemical techniques in geothermal exploration. In: D'Amore, F. (editor), *Applications of geochemistry in geothermal reservoir development*. UNITAR/UNDP, Rome, Italy, 119-144.

Grant, M.A., Donaldson, I.G., and Bixley, P.F., 1982: *Geothermal reservoir engineering*. Academic Press, NY, 369 pp.

Halldórsdóttir, S., Björnsson, H., Axelsson, G., Gudmundsson, A., and Mortensen, A.K., 2010: Temperature model and volumetric assessment of the Krafla geothermal field in N-Iceland. *Proceedings of the World Geothermal Congress 2010, Bali, Indonesia*, 10 pp.

Horne, R.N., 1995: *Modern well test analysis, a computer aided approach* (2nd ed.). Petroway Inc., USA, 257 pp.

James, R., 1970: Factors controlling borehole performance. *Geothermics, Sp. issue, 2-2,* 1502-1515.

Jónsson, P., 2011: *Injection well testing*. UNU-GTP, Iceland, unpublished lecture notes.

Júlíusson, E., Grétarsson, G., and Jónsson, P., 2010: *Well Tester.1.0b. User´s guide*. ISOR – Iceland GeoSurvey, report 2008/63, 26 pp.

Karingithi, C.W., 2000: Geochemical characteristics of the Greater Olkaria geothermal field, Kenya. Report 9 in: *Geothermal Training in Iceland 2000.* UNU-GTP, Iceland, 165-188.

Karingithi, C.W., 2002: *Hydrothermal mineral buffers controlling reactive gases concentration in the Greater Olkaria geothermal system, Kenya*. University of Iceland, MSc thesis, UNU-GTP, Iceland, report 2, 61 pp.

Kariuki, M.N., 2003: Reservoir assessment and wellbore simulations for the Olkaria Domes geothermal field, Kenya. Report 14 in: *Geothermal training in Iceland 2003*. UNU-GTP, Iceland, 337-360.

Lagat, J.K., 1995: Geology, hydrothermal alteration and fluid inclusion studies of the Olkaria Domes geothermal field, Kenya. Report 5 in: *Geothermal training in Iceland 1995*. UNU-GTP, Iceland, 135-154.

Lagat, J.K., 2004: *Geology, hydrothermal alteration and fluid inclusion studies of the Olkaria Domes geothermal field, Kenya.* University of Iceland, MSc thesis, UNU-GTP, Iceland, report 1, 79 pp.

Lichoro, C.M., 2009: Joint 1-D inversion of TEM and MT data from Olkaria Domes geothermal area, Kenya. Report 16 in: *Geothermal training in Iceland 2009*. UNU-GTP, Iceland, 289-318.

Malimo, S.J., 2009: Interpretation of geochemical well test data for wells OW 903B, OW 904B and OW 909 Olkaria domes, Kenya. Report 17 in: *Geothermal training in Iceland 2009*. UNU-GTP, Iceland, 319-344.

Mariita, N.O., 2010: Exploration history of Olkaria geothermal field by use of geophysics. *Presentation at Short Course V on Exploration for Geothermal Resources, UNU-GTP, KenGen, and GDC, Lake Bogoria and Lake Naivasha, Kenya,* 13 pp.

Muchemi, G.G., 2000: *Conceptualized model of Olkaria geothermal field.* The Kenya Electricity Generating Company, Ltd, internal report, 13 pp.

Mungania, J., 1992: *Preliminary field report on geology of Olkaria volcanic complex with emphasis on Domes area field investigations*. Kenya Power Company internal report.

Mwangi M.N., and Bromley, 1986: *A review of geophysical model of Olkaria geothermal field.* Kenya Power Company, internal report no. GF/OW/012.

Mwarania, F.M., 2010: A reservoir assessment of the southeast part of Olkaria Domes geothermal field, Kenya. Report 22 in: *Geothermal training in Iceland 2010*. UNU-GTP, Iceland, 417-440.

Naylor, W.I., 1972: *Geology of the Eburru and Olkaria prospects.* U.N. Geothermal Exploration Project, report.

Odeny, O.N.J., 1999: Analysis of the downhole data and preliminary production capacity estimate for the Olkaria Domes geothermal field, Kenya. Report 11 in: *Geothermal training in Iceland 1999*. UNU-GTP, Iceland, 285-306.

Ofwona, C.O., 2002: *A reservoir study of Olkaria East geothermal system, Kenya.* University of Iceland, MSc thesis, UNU-GTP, Iceland, report 1, 86 pp.

Omenda, P.A., 1998: The geology and structural controls of the Olkaria geothermal system, Kenya. *Geothermics, 27-1*, 55-74.

Opondo, K.M., 2007: *Corrosive species and scaling in wells at Olkaria and Reykjanes, Svartsengi and Nesjavellir, Iceland.* University of Iceland, MSc thesis, UNU-GTP, Iceland, report 2, 73 pp.

Pruess, K., Oldenburg, C., and Moridis, G., 1999: *TOUGH2 users guide version 2.0,* Lawrence Berkeley National Laboratory, 197 pp.

Shackleton, R.M., 1986: Precambrian collision tectonics in Africa. In: Coward, M.P., and Ries, A.C. (eds.), *Collision tectonics.* Geol. Soc., Spec. Publ. 19, 329-349.

Simiyu, S.M., Oduong, E.O., and Mboya, T.K., 1998: *Shear wave attenuation beneath the Olkaria volcanic field*. KenGen, internal report, 30 pp.

Stefánsson, V., and Steingrímsson, B.S., 1990: *Geothermal logging I, an introduction to techniques and interpretation* (3rd edition). Orkustofnun, Reykjavík, report OS-80017/JHD-09, 117 pp.